

# Development of a Polo-like Kinase-1 Polo-Box Domain Inhibitor as a Tumor Growth Suppressor in Mice Models

Pethaiah Gunasekaran,<sup>††</sup> Min Su Yim,<sup>††</sup> Mija Ahn, Nak-Kyun Soung, Jung-Eun Park, Jaehi Kim, Geul Bang, Sang Chul Shin, Joonhyeok Choi, Minkyong Kim, Hak Nam Kim, Young-Ho Lee, Young-Ho Chung, Kyeong Lee, Eunice EunKyeong Kim, Young-Ho Jeon, Min Ju Kim, Kyeong-Ryoon Lee, Bo-Yeon Kim, Kyung S. Lee,<sup>\*</sup> Eun Kyoung Ryu,<sup>\*</sup> and Jeong Kyu Bang<sup>\*</sup>

Cite This: <https://dx.doi.org/10.1021/acs.jmedchem.0c01451>

Read Online

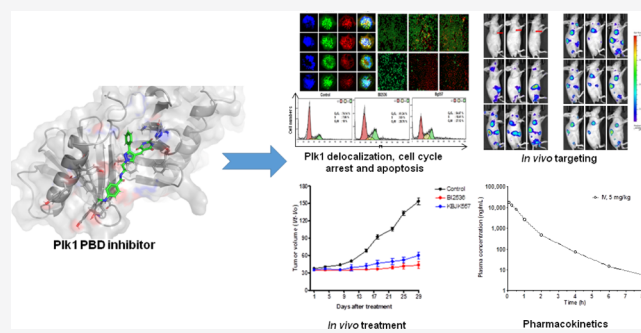
ACCESS |

Metrics & More

Article Recommendations

Supporting Information

**ABSTRACT:** Polo-like kinase-1 (Plk1) plays a key role in mitosis and has been identified as an attractive anticancer drug target. Plk1 consists of two drug-targeting sites, namely, N-terminal kinase domain (KD) and C-terminal polo-box domain (PBD). As KD-targeting inhibitors are associated with severe side effects, here we report on the pyrazole-based Plk1 PBD inhibitor, KBJK557, which showed a remarkable *in vitro* anticancer effect by inducing Plk1 delocalization, mitotic arrest, and apoptosis in HeLa cells. Further, *in vivo* optical imaging analysis and antitumorigenic activities in mouse xenograft models demonstrate that KBJK557 preferentially accumulates in cancer cells and selectively inhibits cancer cell proliferation. Pharmacokinetic profiles and partition coefficients suggest that KBJK557 was exposed in the blood and circulated through the organs with an intermediate level of clearance ( $t_{1/2}$ , 7.73 h). The present investigation offers a strategy for specifically targeting cancer using a newly identified small-molecule inhibitor that targets the Plk1 PBD.



## INTRODUCTION

Understanding the protein–protein interaction and their binding sites are considered as an important tool for developing novel therapeutics. Polo-like kinases (Plks) are a class of serine/threonine protein kinases (classified into Plk1–5) that mediate nonoverlapping roles in various cellular processes critical for cell proliferation.<sup>1–5</sup> Among them, Plk1 plays essential roles during the multiple stages of M-phase progression, including mitotic initiation, centrosome maturation, bipolar spindle formation, chromosome segregation, and cytokinesis.<sup>6</sup> Remarkably, overexpression of Plk1 appears to be required for the viability of cancer cells bearing oncogenic Ras and inactivated p53 mutation(s) but not their isogenic wild-type (WT) cells.<sup>7</sup> Moreover, interfering with the Plk1 function induces mitosis arrest and subsequent apoptosis and retards tumor growth.<sup>7–9</sup> Therefore, specific inhibition of Plk1 has been considered an attractive strategy for anticancer therapy.

Plk1 comprises two drug target sites, namely, N-terminal catalytic domain, especially the ATP-binding site, and the C-terminal polo-box domain (PBD). For the past few decades, a significant amount of work has been carried out to develop various Plk1 inhibitors, primarily targeting the N-terminal ATP-binding site. For instance, a dihydropteridinone-derived inhibitor, BI-2536, and its derivative, volasertib (BI 6727), were developed by Boehringer Ingelheim. Although they have

been widely tested under various preclinical and clinical settings, their usage has been limited because of their dose-limiting toxicities<sup>10</sup> that may stem from cross-reactivity with closely related kinases, including Plk2 and Plk3.<sup>11–13</sup> As Plk2 and Plk3 act as tumor suppressors,<sup>14</sup> selective inhibition of Plk1 is an essential requirement to be an efficient anticancer agent.

Unlike the kinase domain (KD), which imposes a grave disadvantage in selectivity because of the existence of a high degree of sequence similarity among related kinases, the C-terminal PBD, a unique protein–protein interaction domain of the Plk subfamily, offers an inherent advantage. Notably, only three PBDs from Plk1, Plk2, and Plk3 appear to show a considerable level of homology, whereas those from Plk4 and Plk5 are considerably different in structure and primary sequence. It is well documented that PBD-dependent subcellular location is critical for the mitotic functions of Plk1.<sup>15</sup> Thus, specific inhibition of the function of Plk1 PBD is

Received: August 20, 2020

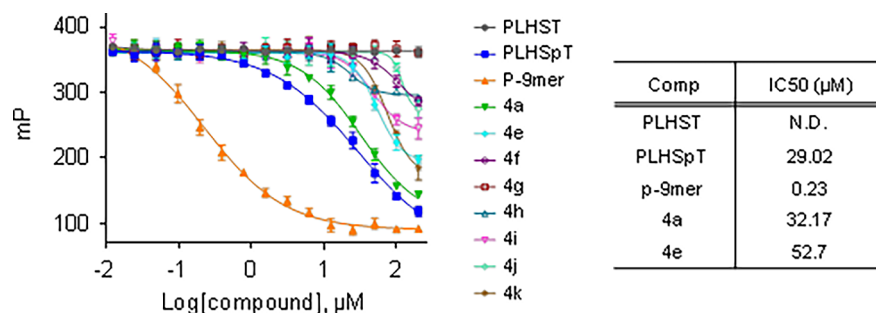
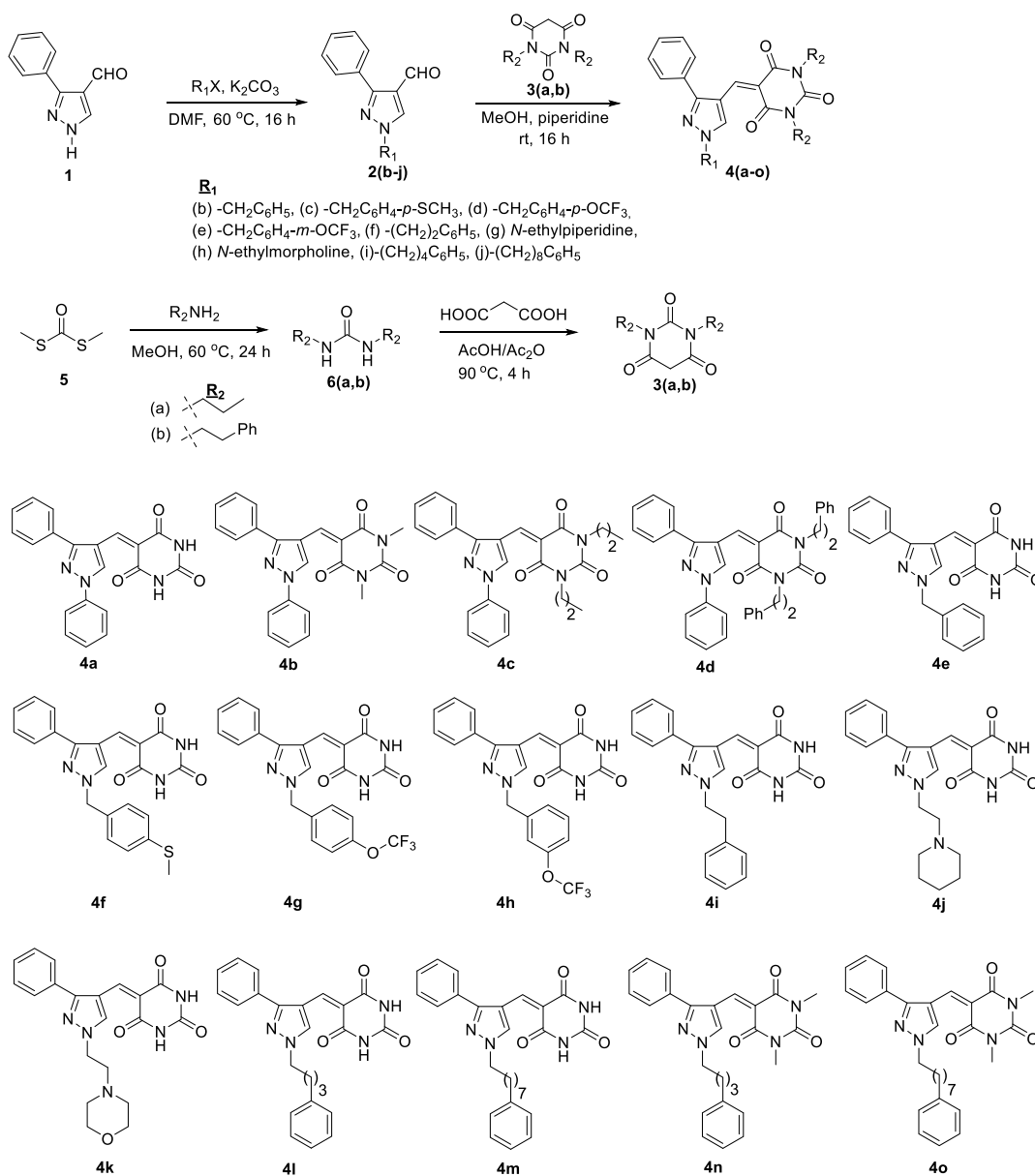


Figure 1. Data obtained with a Plk1 PBD-specific FP-based assay.

### Scheme 1. Synthesis and Structures of 4(a–o)

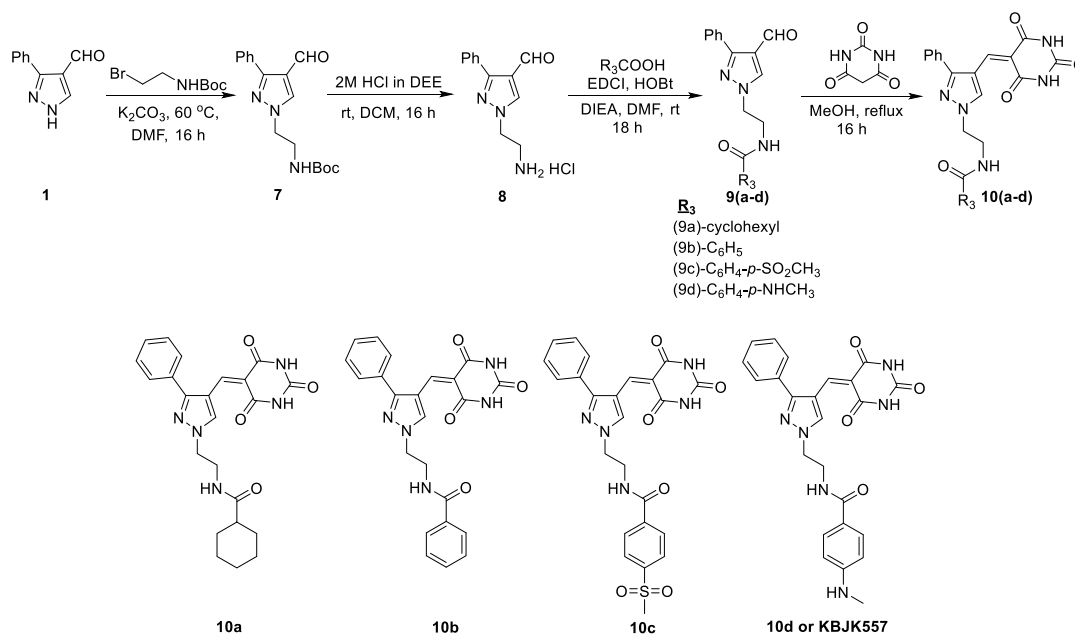


considered as an attractive therapeutic strategy for treating cancer, as it would trigger the G2/M cell cycle arrest and subsequent apoptosis in tumor cells.<sup>16–18</sup>

Although various studies reported the minimal peptide, PLHSpT, and its derivatives as novel peptide-based inhibitors,<sup>19–21</sup> they have severe drawbacks, such as proteolytic

instability and poor cell permeability. To overcome the disadvantages of peptide inhibitors, small molecular inhibitors such as poloxin,<sup>22,23</sup> poloxin-2,<sup>9</sup> poloxipan, purpurogallin (PPG),<sup>24</sup> thymoquinone (TQ),<sup>22</sup> green tea catechins,<sup>25</sup> and others<sup>26,27</sup> were identified. Even though TQ,<sup>26</sup> poloxin,<sup>23</sup> and T521<sup>27</sup> were tested for the inhibition of tumor growth *in vivo*,

Scheme 2. Synthesis of Second-Phase Derivatives



the cancer-targeting ability of these inhibitors using imaging studies in a mouse xenograft model was not investigated yet. Moreover, these inhibitors were not identified through an extensive structure–activity relationship (SAR) study.

The present study, which identified a pyrazolopyrimidine-fused small molecule as a new chemical scaffold against Plk1 PBD, makes several significant advances over other reported Plk1 PBD inhibitors. First, the most active compound, KBJK557, obtained through extensive SAR studies, displayed an appreciable level of Plk1 PBD selectivity and cell permeability. Second, KBJK557 effectively delocalized Plk1 and induced cell cycle arrest and apoptosis in cancer cells. Third, KBJK557 conjugated with cyanine-5 showed cancer-targeting ability in an *in vivo* mouse xenograft model. Fourth, intravenously injected KBJK557 displayed a significant effect in inhibiting cancer growth in a mouse xenograft model with a low dosage level. To the best of my knowledge, this is the first study reporting a small-molecule scaffold against Plk1 PBD that exhibits antitumor activities in a mouse xenograft model with significant pharmacokinetic profiles.

## RESULTS

**Design, Virtual Screening, and Synthesis.** To identify a core moiety for developing the Plk1 PBD inhibitor, we performed virtual screening with a library of compounds as described in methods and found that 1,3,4-trisubstituted pyrazole core skeleton **4a** was a most potent hit compound (Figure 1). To derivatize the core residue, we carefully investigated the crystal structure of Plk1 PBD in complex with the most potent minimal peptide 4J (PDB ID 3RQ7).<sup>20</sup> It is inferred from the crystal structure that interactions at three major binding pockets (broad pyrrolidine binding, deep and narrow tyrosine-rich channel, and phosphate-binding pocket) determine the binding affinity and selectivity. In particular, the broad pyrrolidine binding pocket, surrounded by Trp414, Phe535, and Arg516, is instrumental in achieving the Plk1 selectivity from two other related Plk2 and Plk3. A deep and narrow tyrosine-rich channel, enclosed by Tyr417, Tyr481, and Tyr485, delivers a high binding affinity >1000-fold; in addition, a

phospho binding pocket, which possesses His538 and Lys540 residues that undergo electrostatic interaction with Plk1 PBD inhibitors.

**First-Phase Synthesis.** Based on the aforementioned preliminary structural prerequisites, we envisioned 1,3,4-trisubstituted pyrazole core residue **4**, which offers the possibility to derivatize various compounds through anchoring alkyl/aryl chains at the pyrazole N1 position and functionalizing the NH of the barbituric acid arylidene tethered at the 4-position of pyrazole. To synthesize **4**, as delineated in Scheme 1, we began with the N-alkylation of 3-phenyl-4-pyrazole carboxaldehyde (**1**) using various aryl/alkyl bromides in the presence of  $K_2CO_3$  in DMF to result in the formation of **2(b–j)**. Further, condensation of various barbituric acids (**3**) with **2** resulted in the formation of **4(a–o)**. To derive substituted barbituric acids **3(a,b)**, different amines were treated with **5** in methanol to yield **6**, which was under treatment with malonic acid in the presence of acetic anhydride and acetic acid, resulting in the formation of **3(a,b)**. After the synthesis, the hit compound **4a** was tested for its ability to inhibit Plk1 PBD using a fluorescence polarization (FP) assay.<sup>20</sup> To accurately assess the level of its inhibitory activity, a previously characterized Plk1 PBD-binding peptide, PLHSpT, and its nonbinding control, PLHST, and a potent PLHSpT-containing p-9mer peptide (Ac-PLHSpTAIYA-NH<sub>2</sub>)<sup>19</sup> were included. A small-molecule Plk1 PBD inhibitor, PPG, known to exhibit a moderate level of anti-Plk1 activity<sup>24</sup> was also included for comparative analysis (Figure S1).

Surprisingly, the hit compound **4a** was found to be more potent than the small-molecule Plk1 PBD inhibitor, PPG (Figure S1), which prompted us to perform a detailed SAR study. Thus, to examine whether the interactions of NH at barbituric acid in **4a** make a significant contribution in Plk1 PBD activity, we introduced methyl, propyl, and ethylphenyl residues at the NH position to generate **4b**, **4c**, and **4d** respectively. Unfortunately, these compounds did not display any Plk1 PBD inhibition (Figure S1). To evaluate the influence of alkyl chain length at the NH position of pyrazole, we introduced benzyl derivatives, including **4e**, **4f** (4-phenyl-*S*-methyl), **4g** (4-phenoxytrifluoromethyl), and **4h** (3-phenoxytrifluoromethyl).

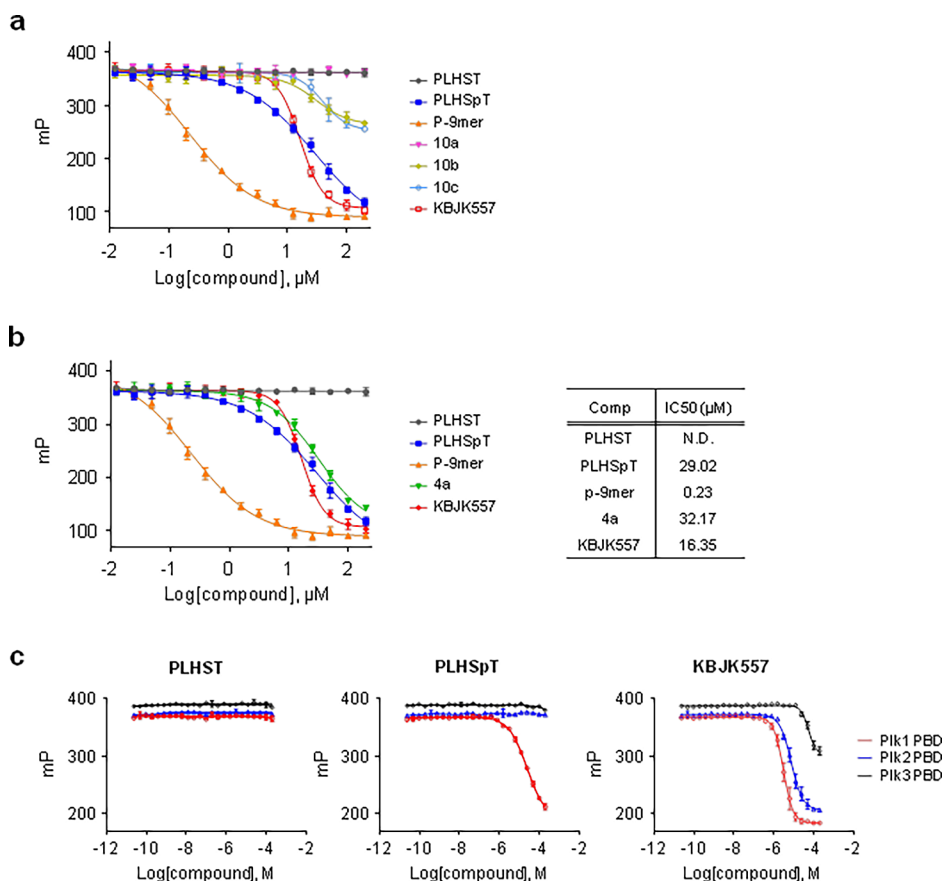


**Figure 2.** Second-phase derivatization: (a) inhibitory effects of second-phase derivatives against Plk1 PBD using an FP-based assay; (b) comparison of FP-based assay results of hit compound **4a** and lead compound KBJK557 with references; (c) evaluation of KBJK557 selectivity against PBD of Plk1, Plk2, and Plk3 using FP-based assays. A Plk1 PBD-binding PLHSpT and its nonphospho parental PLHST<sup>19</sup> were used as positive and negative controls, respectively. KBJK557 showed IC<sub>50</sub> = 3.05 μM (PBD1) and 7.52 μM (PBD2).

These compounds did not show considerable Plk1 PBD inhibition (Figure 1). Further increment in the *N*-alkyl chain length resulted in ethylphenyl (**4i**), *N*-ethylpiperidine (**4j**), and *N*-ethylmorpholine (**4k**). Among them, **4k** displayed Plk1 PBD inhibition (IC<sub>50</sub> = 71.03 μM); however, it was less than that of the hit compound **4a** (IC<sub>50</sub> = 32.17 μM). This binding affinity may be attributed to the presence of heteroatoms, which might have undergone polar interactions with PBD-binding sites. Further increase in chain lengths using four- and eight-carbon linkers yielded **4l**, **4m**, **4n**, and **4o**, respectively. Surprisingly, **4l** showed appreciable Plk1 PBD inhibition (Figure S1).

**Second-Phase Derivatization.** From the above results, especially from **4k** and **4l**, we speculated that a four-carbon intervening chain attached at pyrazole nitrogen and the presence of heteroatoms may yield an inhibitor with a significant Plk1 PBD-binding affinity. Furthermore, the amide linker could be an optimal choice for synthesizing the derivatives, as shown in Scheme 2. Initially, to perform the *N*-alkylation on pyrazole aldehyde (**1**), *N*-Boc-bromoethylamine was treated in the presence of K<sub>2</sub>CO<sub>3</sub> in DMF to yield **7**, further treatment of which with 2 M HCl in diethyl ether resulted in the formation of amine hydrochloride, **8**. To derive amide derivatives **9(a–d)**, various acids were treated with amine hydrochloride (**8**) in the presence of 1-ethyl-3-(3-dimethylaminopropyl)carbodiimide (EDCI), 1-hydroxybenzotriazole (HOBt), and *N,N*-diisopropylethylamine (DIEA). Finally, condensation of barbituric acid with **9(a–d)** in methanol under reflux conditions yielded **10(a–d)**.

Initially, we synthesized **10a**, in which pyrazole nitrogen and a cyclohexyl are separated by four intervening atoms, including an amide linkage. Similarly, to examine the influence of aromatic substituents, we synthesized **10b** by replacing the cyclohexyl group with a phenyl moiety in **10a**. Unfortunately, as shown in Figure 2a, the assay results of both compounds did not reveal significant binding affinity. Further, to validate the effects of polar substituents in **10b**, we introduced methane sulfonyl and *N*-methyl substituents at the para position of phenyl in **10b**, yielding **10c** and **10d** (KBJK557), respectively. Unfortunately, **10c** did not show any binding affinity; in contrast, KBJK557 was found to be the most potent Plk1 PBD inhibitors among the derived compounds with a binding affinity of IC<sub>50</sub> = 16.35 μM, which was more potent than that of the Plk1 PBD inhibitor minimal peptide, PLHSpT (IC<sub>50</sub> = 29.02 μM) (Figure 2b), and the hit compound, **4a** (IC<sub>50</sub> = 32.17 μM).

Collectively, through this SAR study, we identified that (i) pyrazole holding *N*-alkyl phenyl derivatives and barbituric acid arylidene with free NH are important for the Plk1 PBD activity; (ii) even though small alkyl chains attached at the NH position of pyrazole showed considerable activity, manipulation of the alkyl chain with four intervening atoms resulted in improvement in the Plk1 PBD affinity; in particular, amide linked with a *p*-aminomethylphenyl group was found to be instrumental in obtaining enhanced Plk1 PBD affinity.

**Impact of KBJK557 on Selectivity.** To examine the binding specificity of KBJK557 against PBDs of closely related Plk1, 2, and 3, we performed a selectivity test in comparison with

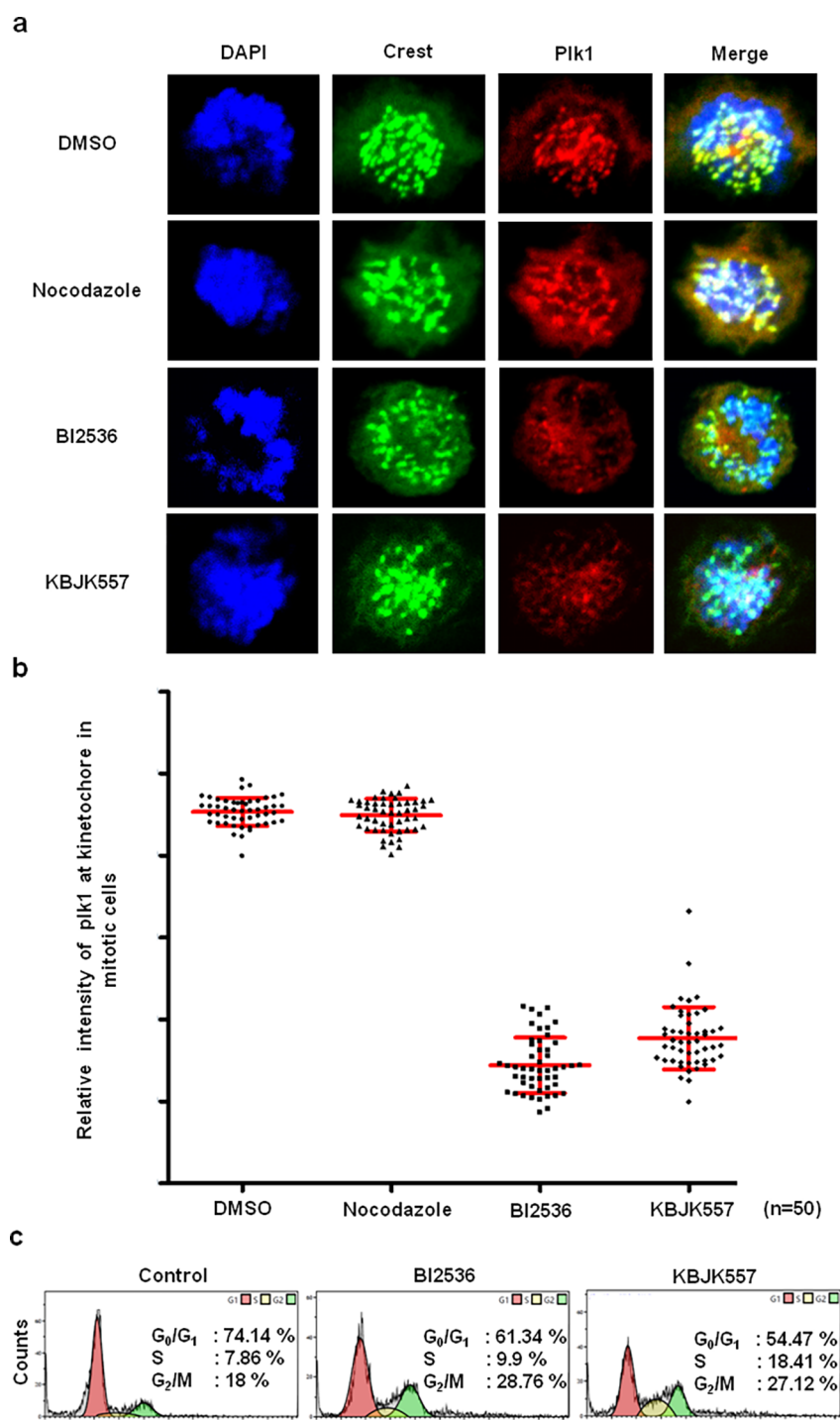


**Figure 3.** Plk1 delocalization at kinetochore and cell cycle arrest. (a) Plk1 signal (red) was observed at the kinetochore (green), which was represented by the anti-crest antibody. Among the mitotic cells, prometaphase cells were captured and analyzed. The cell phase was judged by the DNA (blue) shape. Cells were treated with DMSO, nocodazole, BI2536, and KBJK557 for 18 h. (b) Relative Plk1 intensity in kinetochore was measured and visualized in a graph. At least 10 kinetochores were measured per cell. The value was shown based on the DMSO sample. The “n” denotes cell number. \*\*\* $p < 0.001$ . (c) Fluorescence-activated cell sorting analysis of cell cycle arrest in HeLa cancer cells after incubation with BI2536 and KBJK557. Cells were cultured for 24 h with BI2536 and KBJK557. Cell cycle arrest was measured by flow cytometry with PI staining.

that of Plk1 PBD-specific PLHSpT.<sup>19,20</sup> As shown in Figure 2c, KBJK557 recognized the Plk1 selectively over Plk3 because it did not bind with Plk3. In the case of the KD targeting inhibitor, BI2536, Plk1 selectivity over Plk3 was approximately 10-fold.<sup>28</sup> Besides, KBJK557 distinguished Plk1 over Plk2 although it was showing a narrow window of difference by twofold. Similarly, this selectivity in the case of BI2536 was threefold.<sup>28</sup> As the

interface between two interacting proteins is often large and the binding site is shallow, achieving both high binding affinity and selectivity by a small molecule is a challenging task. However, KBJK557 showed great selectivity for Plk1 PBD over PBD3 (Figure 2c) and Plk2 is expressed only in the G1 stage of the cell cycle.<sup>29</sup> Thus, the effect of KBJK557 on the cell cycle and proliferation (below) is likely caused by inhibiting Plk1 PBD.

**Disruption of Plk1 Localization by KBJK557.** To determine the ability of KBJK557 to interfere with the function of Plk1 PBD, we examined the intracellular localization capacity of Plk1 after treating the cells with KBJK557. BI2536, a well-characterized ATP inhibitor against Plk1, was included for comparison. To this end, asynchronously growing HeLa cells were treated with either control DMSO or KBJK557 for 18 h, immunostained, and subjected to confocal imaging analysis (Figure 3a). Quantification of Plk1 intensities at kinetochores showed that the Plk1 signal (red) was strong in both DMSO and nocodazole-treated samples. In contrast, the Plk1 signal was effectively ( $\sim 60.95\%$ ) decreased in cells treated with KBJK557. Cells treated with BI2536 also substantially ( $\sim 68.21\%$ ) reduced the level of Plk1 localized to the mitotic kinetochore (Figure 3b). This is not surprising because Plk1 catalytic activity is required to localize to kinetochores through a mechanism called self-priming and binding.<sup>1</sup> Collectively, these results strongly suggest that KBJK557 delocalizes Plk1 from its endogenous localization sites by competitively blocking Plk1 PBD from binding to its targets at the kinetochore.

**Effect of KBJK557 on the Cell Cycle.** Next, we analyzed the effect of KBJK557 on cell cycle progression in HeLa cells using flow cytometry analysis. HeLa cells were treated with KBJK557 and BI2536 for 24 h. Interestingly, cells treated with KBJK557 induced a partial but significant G2/M arrest (compare 27% with 18% observed in control cells) at a level similar to that of BI2536 (Figure 3c). Notably, KBJK557 also significantly delayed S-phase progression, as indicated by  $\sim 11\%$  increase of the cell population at this stage.

**Effect of KBJK557 on the Plk1 PBD–Cdc25C Interaction.** Plk1 PBD plays a key role in promoting mitotic entry at the G2/M phase of the cell cycle by phosphorylating and activating Cdc25C through its PBD-dependent interaction.<sup>30</sup> Therefore, we directly examined whether KBJK557 can inhibit the interaction between Plk1 PBD and its phosphorylated binding target, p-Cdc25C. The GST-PBD H538A K540M (AM) mutant defective in recognizing its phosphorylated targets<sup>31</sup> was used as a control. As shown in Figure S2, WT PBD effectively interacted with phosphorylated Cdc25C, whereas its respective AM mutant did not. Under these conditions, KBJK557 substantially diminished the level of phosphorylated Cdc25C coprecipitated with GST-Plk1 PBD. These results confirm that KBJK557 has a capacity to competitively inhibit Plk1 PBD-dependent interaction against its binding targets.

**Induction of Apoptotic Cell Death in Cancer Cells.** The ability of KBJK557 to specifically inhibit PBD-dependent interaction and induce a partial G2/M arrest prompted us to investigate whether it can induce apoptosis in HeLa cells. In a fluorescence apoptosis assay that shows live cells in green and dead cells in red color (Figure 4a), we observed that treatment of HeLa cells with KBJK557 resulted in a significant level of apoptotic cell death (24.6% at 24 h and 71.1% at 48 h). Under these conditions, BI2536 induced slightly more apoptotic cell death than KBJK557 (31.1% at 24 h and 91.5% at 48 h) (Figure 4b).

**Cellular Uptake of the Fluorescence-Conjugated Inhibitor.** To assess the cellular uptake of KBJK557 *in vitro*, we performed fluorescence imaging analysis using Cy5-conjugated KBJK557 (Scheme S2). As shown in the confocal microscopic scanning image (Figure S3), Cy5-conjugated KBJK557 (red) colocalized with DAPI-stained chromosomes (arrows), suggesting that KBJK557 penetrated the cytosol and

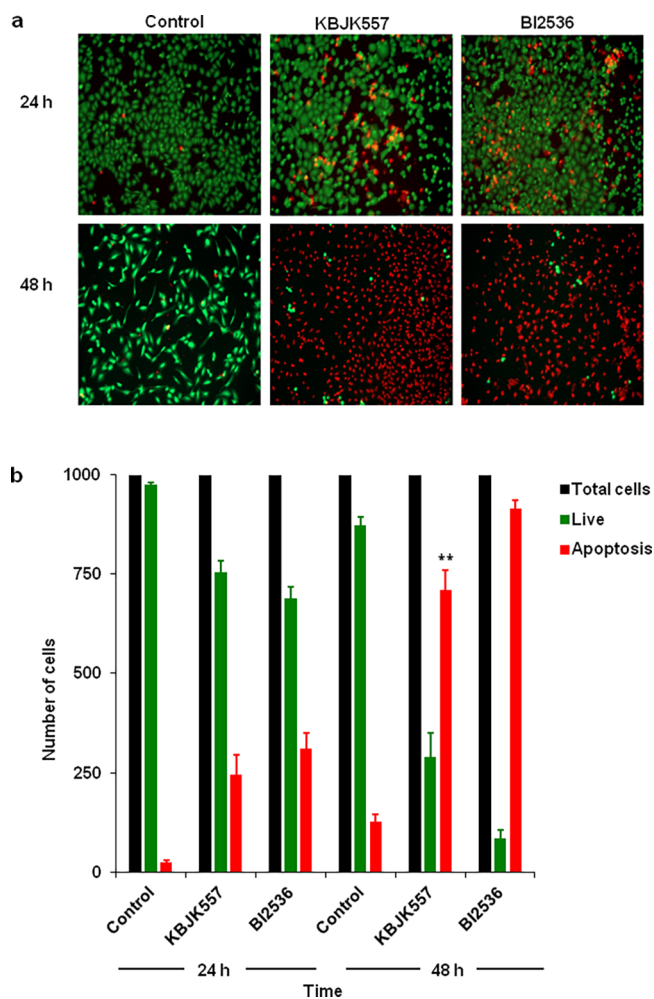


**Figure 4.** Induction of apoptosis in HeLa cells by KBJK557. (a) Cells were treated with BI2536 and KBJK557 for 24 h. Green color indicates live cells and red color indicates dead cells. (b) Number of live or dead cells is shown by a bar graph. All images were observed using a fluorescence microscope (100 $\times$  magnification). \*\* $p < 0.01$ .

reached the nucleus. These results confirm that our compound can penetrate the cell membrane *in vitro*, which paves the way for the possibility to perform the *in vivo* tumor-targeting studies.

**Optical Imaging Probe for Tumor Diagnosis.** In order to analyze the *in vivo* tumor-targeting efficacy of KBJK557, tumor-bearing mice were injected with the Cy5-conjugated KBJK557 (Scheme S2) via a tail vein and subjected to optical imaging analysis. Fluorescence imaging was carried out at 6, 24, 30, and 48 h after injecting the compound. Strikingly, we observed that tumors emerging from the HeLa cell xenografts exhibited a significant fluorescent signal along with organs, including liver, kidney, heart, and spleen. This is not surprising because drugs are easily distributed in these highly perfused organs. In addition, a higher level of uptake in the liver and kidney can also be attributable to the fact that drug elimination occurs through these organs. However, the signal intensities of most of the organs were found to decrease gradually in a time-dependent manner (Figure 5a). The quantitative evaluation of tumor and muscle fluorescence intensity showed that the fluorescence intensity of tumor ( $1.75 \pm 0.12 \times 10^9$  p/s/cm<sup>2</sup>/sr) was  $\sim 4.2$ -fold higher than that of muscle ( $4.18 \pm 0.24 \times 10^8$  p/s/cm<sup>2</sup>/sr) at 48 h (Figure 5b). The finding that KBJK557 was significantly accumulated in tumors but not in the surrounding normal

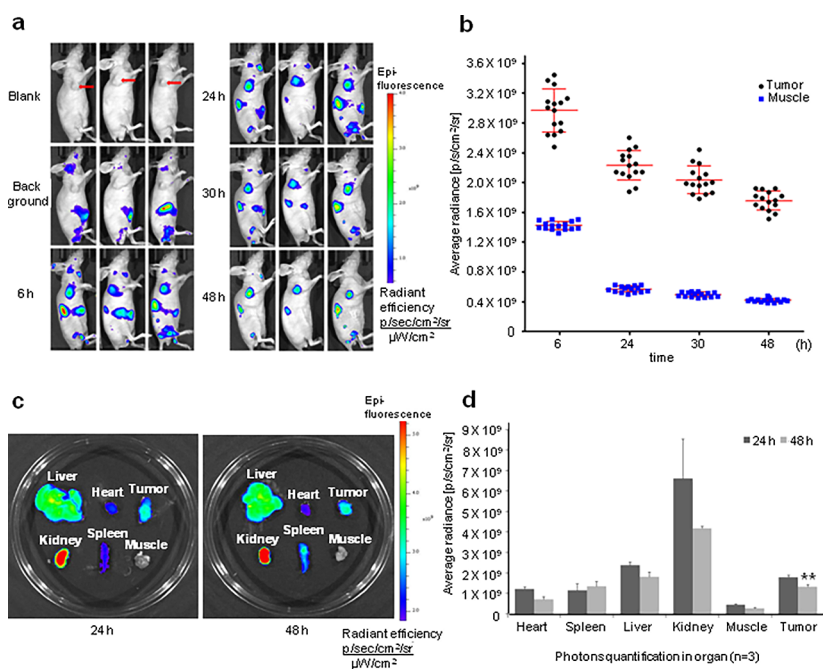


**Figure 5.** Fluorescence images of Cy5-conjugated KBJK557 in HeLa tumor-bearing mice. (a) Fluorescence images were obtained at 6, 24, 30, and 48 h after injection of Cy5-conjugated KBJK557 (5 mg/kg body weight/200  $\mu\text{L}$ ). Red arrows indicated tumors of mice. (b) ROI analysis of fluorescence intensity in tumors and muscles from fluorescence images. Mice tumors were measured in at least five points. The “*n*” means mice number. (c) After *in vivo* fluorescence images, mice were sacrificed and *ex vivo* fluorescence images were obtained (24 and 48 h). (d) Fluorescence intensity in organs and the tumor were measured at 24 and 48 h. Values represent mean average radiance and the error bars represent SDs. Significant differences at  $**p < 0.01$  (unpaired two-tailed *t*-test).

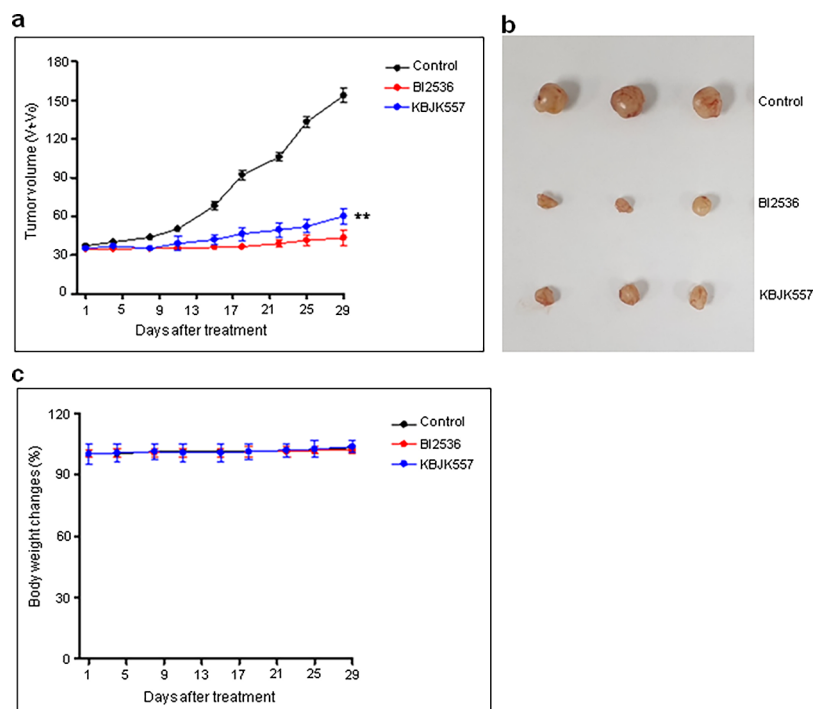


**Figure 6.** *In vivo* anticancer effect of KBJK557 in a xenograft mice model. (a) Tumor volume changes after the treatment of BI2536 and KBJK557 (5 mg/kg body weight) for 29 days. Tumor size was monitored and measured at 3–4-day intervals.  $**p < 0.01$  (unpaired two-tailed *t*-test). Values represent the average  $\pm$  SEM ( $n = 3$  per group). Tumor volume =  $V_t$  (measurement of the tumor volume) –  $V_0$  (initial tumor volume). (b) Following the injection of BI2536 and KBJK557 for 29 days, tumors were harvested. (c) Bodyweight changes (%). The average body weight changes were determined in the control, BI2536-, and KBJK557-treated groups in the cancer xenograft mice model during 29 days.

tissues and slowly perfused tissues, such as muscles (Figure 5a), suggests that KBJK557 has a level of tendency to accumulate in tumor tissues. Consistent with this notion, the ratios of a tumor

to muscle were found to be 2.1-, 3.9-, and 4.11-fold at 6, 24, and 30 h, respectively (Figure 5b). In preinjection fluorescence images, the fluorescence signals that appeared in the peritoneum

of mice were due to the feed, which was found to decrease slowly over time because of the fasting after the injection.

To further investigate the biodistribution of Cy5-conjugated KBJK557, the mice were sacrificed and samples were collected at 24 and 48 h after the injection (Figure 5c). The biodistribution studies revealed that the fluorescence intensity of the liver, kidney, spleen, and tumor was manifest. In addition, the region of interest (ROI analysis) of tumors were  $1.78 \pm 0.09 \times 10^9$  p/s/cm<sup>2</sup>/sr at 24 h and  $1.31 \pm 0.11 \times 10^9$  p/s/cm<sup>2</sup>/sr at 48 h, respectively (Figure 5d). These results further support our view that Cy5-conjugated KBJK557 exhibits a tendency to accumulate in tumor cells and tissues. Moreover, significant accumulation of KBJK557 in tumor cells suggests that Cy5-conjugated KBJK557 has a potential to be further developed as a tumor diagnostic agent.

#### Anticancer Effect of KBJK557 in Tumor-Bearing Mice.

Inspired by the tumor-targeting ability, KBJK557 was examined for its chemotherapeutic ability in mice bearing HeLa cell xenograft tumors, which were treated with PBS, BI2536, and KBJK557 for 29 days ( $n = 3$ ). The tumor growth of the BI2536- and KBJK557-treated group was remarkably reduced compared to that of the PBS-treated group (Figure 6a,b). The tumor sizes in the PBS-treated group were increased to  $68.36 \pm 2.97$ ,  $106.05 \pm 3.08$ , and  $153.57 \pm 5.64$  mm<sup>3</sup> after 15, 22, and 29 days, respectively. In contrast, both BI2536- and KBJK557-treated groups showed tumor sizes substantially smaller than those of the control PBS-treated group. The highest antitumor effect of KBJK557 (60.78%) was observed on the 25th day of treatment, compared with the control group. To further verify that the reduction of tumor size is not due to the stress and external factors, we examined the body weight in all three groups and found no dramatic changes (Figure 6c). Taken together, these results suggest that KBJK557 exhibits an antitumorigenic activity, which could be attributable to its selective tumor-targeting ability but not surrounding normal tissues (Figure 5). Its ability to antagonize Plk1 localization and function and its antitumorigenic effect in a mouse xenograft model demonstrate that KBJK557 has a great potential to become a model compound for developing anti-Plk1 PBD agents.

**Pharmacokinetics.** To evaluate the relative safety of employing KBJK557 *in vivo*, we performed pharmacokinetic studies using rodents and the pharmacokinetic profile of the compound was examined. Male ICR mice were used and the blood samples were collected at 0.08, 0.25, 0.5, 1, 2, 4, 6, 8, and 24 h after intravenous administration at a dose of 5 mg/kg. The blood samples were centrifuged immediately after collection and the concentrations of the plasma fractions were determined using an Agilent LC-MS/MS system (Figure 7). The pharmacokinetic profiles of KBJK557 were obtained by noncompartmental analysis (Table 1). The organ tissues (i.e., liver, spleen, and kidney) were isolated at 2, 6, and 24 h after intravenous administration at a dose of 5 mg/kg. Intravenous injection of KBJK557 resulted in the intermediate level of clearance (CL, 0.43 L/h/kg), half-life ( $t_{1/2}$ , 7.73 h), and sufficient systemic exposure (AUC, 11.5  $\mu$ g·h/mL) in the body. The partition coefficients were evaluated as 0.166, 0.045, and 0.182 in liver, spleen and kidney, respectively, which was calculated by the ratio of AUC<sub>last</sub> for each tissue and plasma. These data suggest that KBJK557 possesses significant pharmacokinetic properties that can be further developed into anticancer therapeutics.

**Pan Assay Interference Compounds.** As our lead compound consists of a Michael acceptor, barbituric acid

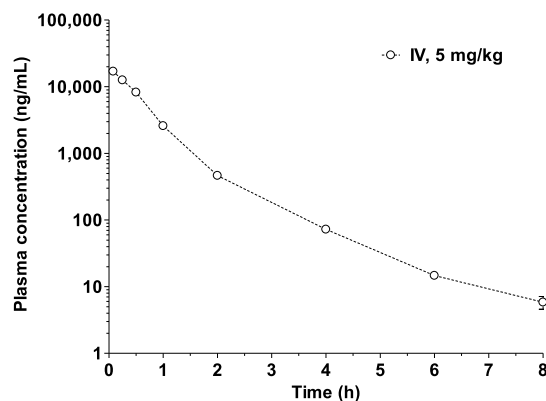


Figure 7. Concentration–time profile of KBJK557 in the mouse plasma after an intravenous administration of KBJK557 (mean  $\pm$  SD,  $n = 5$ ).

Table 1. Pharmacokinetic Profiles of KBJK557 (Mean  $\pm$  SD)

parameters	I.V. (5 mg/kg)
AUC <sub>last</sub> (h·ng/mL)	11,504.31 $\pm$ 369.10
AUC <sub>∞</sub> (h·ng/mL)	11,535.29 $\pm$ 371.69
$t_{1/2}$ (h)	7.73 $\pm$ 0.46
CL (L/h/kg)	0.43 $\pm$ 0.01
$V_{ss}$ (L/kg)	0.31 $\pm$ 0.04
MRT (h)	0.72 $\pm$ 0.10

arylidene, categorized as a substructure of pan assay interference compounds (PAINS),<sup>32</sup> we analyzed the PAINS using <http://zinc15.docking.org/>. As expected, the alkene was found to show PAINS during the evaluation. Thus to verify this aspect, we evaluated KBJK557's anti-Plk1 PBD activity in the presence of L-Cys (Figure 8), whose thiols would react with activated

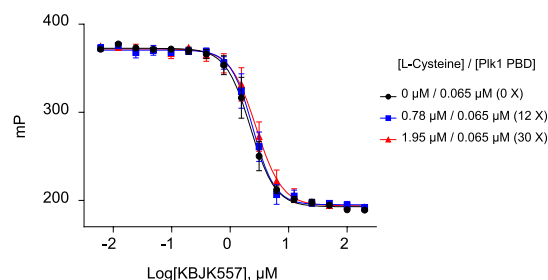
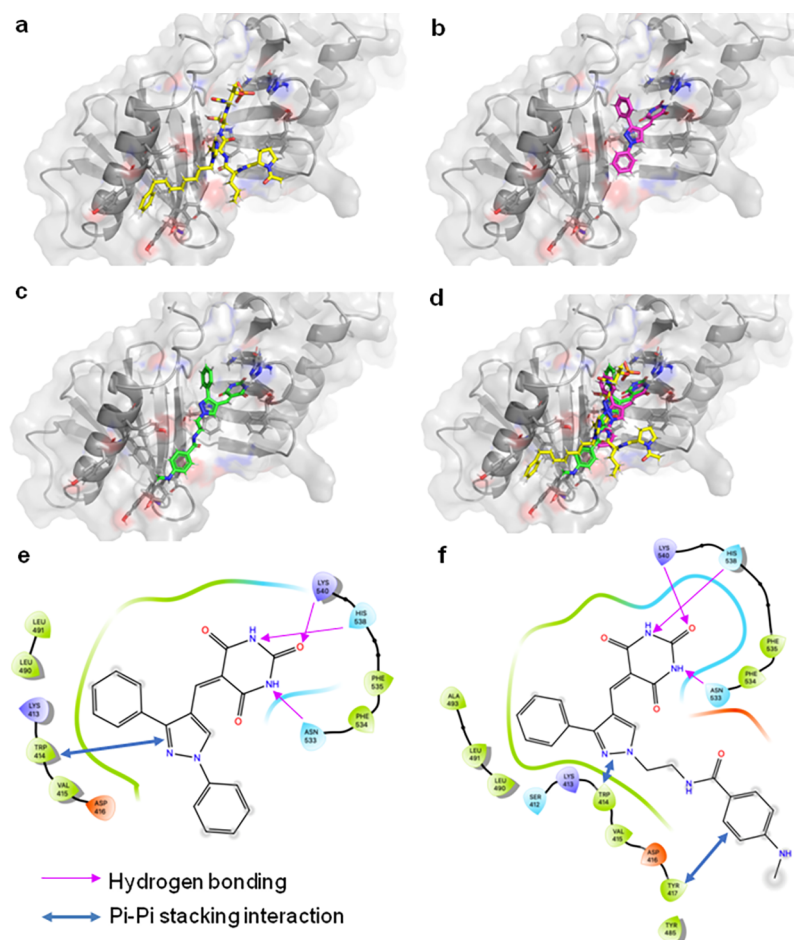


Figure 8. FP assays with L-cysteine. millipolarization (mP) values were determined 30 min after incubation. Data were plotted using GraphPad Prism software.

Michael acceptors. The result showed, however, that L-Cys failed to diminish KBJK557's anti-Plk1 PBD activity, even when it was provided at 30-fold higher concentration than PBD (Figure 8). This result suggests that KBJK557 does not behave like PAINS molecules; instead, it inhibits Plk1 PBD through specific interaction.

**Molecular Modeling.** After virtual screening, in view of understanding the molecular interactions responsible for the Plk1 PBD inhibitory effect, we performed molecular docking studies with the initial hit compound, **4a**, using the UCSF DOCK6.9 program (Figure 9). The results revealed that trioxotetrahydropyrimidin (barbituric acid arylidene) in **4a** could undergo tight electrostatic interactions with the His538, Lys540, and Asn533 residues present in the PBD lattice. Further, pyrazole in **4a** involved in  $\pi$ - $\pi$  stacking interactions with



**Figure 9.** Modeling structures of Plk1 PBD with the (a) 3RQ7 ligand (PDB ID 3RQ7),<sup>20</sup> (b) hit compound **4a**, (c) KBJK557, (d) overlaid structures of the 3RQ7 ligand, **4a**, and KBJK557, (e) interacting sites of **4a** in Plk1 PBD, and (f) interacting sites of KBJK557 in Plk1 PBD. Modeling was done using the DOCK6.9 program.

Trp414. In the subsequent docking analysis with the most potent molecule KBJK557, we also found that trioxotetrahydropyrimidin (barbituric acid arylidene) and pyrazole in KBJK557 engage in electrostatic interactions with His538, Lys540, and Asn533 and  $\pi$ - $\pi$  stacking interactions with Trp414, respectively. Additionally, the alkyl tail attached to the N1 of pyrazole projected toward the tyrosine-rich channel. The phenyl group in the alkyl tail engaged in a  $\pi$ - $\pi$  stacking interaction with Tyr417, which might have contributed to the enhanced anti-Plk1 PBD activity. These three interaction patterns are similar to those observed with the 3RQ7 ligand in Plk1 PBD.

## DISCUSSION AND CONCLUSIONS

Overexpression of Plk1 is predominant in many cancer cells; thus Plk1 is considered a valid target for developing anticancer therapeutics. As Plk1 KD inhibitors developed so far largely exhibit a high level of side effects because of their cross-reactivities, PBD has drawn a lot of attention as an alternative target for anti-Plk1 drug discovery. Even though peptide-based inhibitors targeting Plk1 PBD showed considerable potency *in vitro*, achieving high *in vivo* efficacy remains challenging because of their poor cell permeability and stability. To date, a very few small-molecule Plk1 PBD inhibitors, including T521,<sup>27</sup> TQ,<sup>29</sup> and poloxin1<sup>23</sup> have been investigated *in vivo*. However, they required high dosage levels to display appreciable effects in cancer treatment. In particular, the sulfonyl-oxazole inhibitor

T521 was reported to show antitumor activity by inhibiting Plk1 PBD selectively by covalent binding. Consequently, it induced defects in centrosome integrity, chromosome alignment, and spindle assembly and subsequent apoptosis in HeLa cells. However, compared to KBJK557, the cancer-targeting ability of T521 is not clear because antitumorigenic activity in a mouse xenograft tumor model was demonstrated by an intratumoral injection method.<sup>27</sup> Moreover, the cancer-targeting ability of the abovementioned Plk1 PBD inhibitors using imaging studies in a mouse xenograft model has not yet been investigated.

The data provided here suggest that a pyrazolopyrimidine-fused small-molecule scaffold offers promising structural and chemical features that can be further exploited for the discovery of a new class of Plk1 PBD inhibitor. At the cellular level, KBJK557 is capable of effectively delocalizing Plk1 from its subcellular localization sites and consequently inducing mitotic arrest and apoptotic cell death in cancer cells. These observations demonstrate that KBJK557 can overcome poor cell permeability commonly associated with peptide-derived Plk1 PBD inhibitors and provide proof of principle that specifically inhibiting PBD-dependent interaction is sufficient to disrupt Plk1 function.

Most of the conventional chemotherapeutic drugs possess severe setbacks in distinguishing the cancer cells from normal cells. Thus, identifying a cancer drug with considerable selectivity toward the cancer cells remains the greatest challenge

in the field of cancer therapy.<sup>33</sup> Here, we show that, in an optical imaging study, Cy5-conjugated KBJK557 significantly accumulated in tumors but not their surrounding normal tissues. The liver, kidney, heart, and spleen also exhibited a significant level of Cy5-KBJK557 uptake. However, the fluorescence intensity gradually decreased in a time-dependent manner. The high-level uptake in the liver and kidney is likely due to the systemic circulation of body metabolite and subsequent elimination through these organs.<sup>34</sup> Spleen tissue accumulation is closely related to the reticuloendothelial system organs.<sup>35,36</sup> In addition, to monitor the effects of KBJK557 *in vivo*, we performed the pharmacokinetics study (Table 1). The pharmacokinetic profiles and partition coefficients suggested the systemic exposure of KBJK557 in the blood, thereby distributing it to the highly perfused organs such as liver, kidney, heart, and spleen after intravenous administration in mouse. The accumulation of KBJK557 in the foreleg xenograft tumors hints that KBJK557 may have a capacity to target tumor sites with a level of selectivity. Consistent with these observations, KBJK557 exhibited a significant level of antitumorigenic activities in a mouse xenograft tumor model, comparable to the well-characterized Plk1 KD inhibitor, BI2536.<sup>28</sup>

In summary, our data suggest that KBJK557 is the first small-molecule Plk1 PBD inhibitor that selectively disrupts PBD-dependent interaction *in vitro* and exhibits a significant level of *in vivo* tumor-targeting and treatment effect. KBJK557 appears to have a great potential to be a model for designing anticancer drugs that show selective cancer-targeting ability by targeting Plk1 PBD.

## EXPERIMENTAL SECTION

**General Chemistry Methods.** All reagents and starting materials were purchased from commercial chemical suppliers (Sigma-Aldrich, TCI and Across Organics) and used as received. All the anhydrous organic solvents of purity greater than 99.9% were purchased from Aldrich and used directly. Thin-layer chromatography (TLC) was performed on Merck aluminum sheets with silica gel 60 F254 and they were visualized by ultraviolet light and staining with KMnO<sub>4</sub>, PMA stain (phosphomolybdic acid), and ninhydrin. For the purification of compounds, column chromatography was performed on Merck silica gel 60 (70–230 mesh or 230–400 mesh). NMR spectra including <sup>1</sup>H and <sup>13</sup>C NMR spectra were recorded on a Bruker DRX-400 and DRX-500 spectrometer. Chemical shifts ( $\delta$ ) are reported in parts per million (ppm) measured relative to an internal standard and coupling constants ( $J$ ) are expressed in hertz (Hz). Mass spectra were recorded using a Shimadzu (MALDI-TOF) mass spectrometer. The cyanine-conjugated compound was purified by preparative reversed-phase high-performance liquid chromatography (RP-HPLC, YL9100, Younglin, Korea) and determined to be >95% pure by analytical HPLC [C<sub>18</sub> column (4.6 × 250 mm)]. Two different linear gradients of 0.05% aqueous TFA (eluent A) and 0.05% TFA in CH<sub>3</sub>CN (10–90 over 30 min, eluent B) were used at a flow rate of 1.5 mL per min at 25 °C.

**General Procedure A for the Synthesis of 2(b–j).** **1-Benzyl-3-phenyl-1H-pyrazole-4-carbaldehyde (2b).** 3-Phenyl-1H-pyrazole-4-carbaldehyde (**1**) (0.67 g, 0.003912 mol) in anhydrous DMF (5 mL) was added slowly to a stirred solution of benzyl bromide (**b**) (0.604 g, 0.00355 mol) and potassium carbonate (1.47 g, 0.01065 mol) in anhydrous DMF (20 mL). After completion of the addition, the temperature was slowly raised to 60 °C and the solution was stirred for 16 h. Then, the reaction mixture was quenched by the addition of water (30 mL) and extracted with ethyl acetate (30 mL × 3). The combined organic extracts were washed with brine (40 mL), dried over Na<sub>2</sub>SO<sub>4</sub>, and evaporated. The crude product was purified by silica gel column chromatography using a hexane/dichloromethane/ethyl acetate (1:1:0.2) mixture to afford **2b** as a white solid (0.67 g, 73%). <sup>1</sup>H NMR (400 MHz, CDCl<sub>3</sub>):  $\delta$  9.95 (s, 1H), 7.96 (s, 1H), 7.84–7.69 (m,

2H), 7.55–7.45 (m, 3H), 7.44–7.38 (m, 3H), 7.38–7.33 (m, 2H), 5.39 (s, 2H). <sup>13</sup>C NMR (101 MHz, CDCl<sub>3</sub>):  $\delta$  185.1, 154.2, 134.6, 133.6, 131.6, 129.1, 129.0, 128.9, 128.8, 128.7, 128.4, 121.3, 56.7. MALDI-TOF *m/z*: calcd for C<sub>17</sub>H<sub>14</sub>N<sub>2</sub>O, 262.11; found, 262.35.

**1-(4-(Methylthio)benzyl)-3-phenyl-1H-pyrazole-4-carbaldehyde (2c).** Compound **2c** was synthesized from 3-phenyl-1H-pyrazole-4-carbaldehyde (**1**), 4-(methylthio)benzyl bromide (**c**) and potassium carbonate by following general procedure A (white solid, 76%). <sup>1</sup>H NMR (400 MHz, CDCl<sub>3</sub>):  $\delta$  9.92 (s, 1H), 7.93 (s, 1H), 7.72 (dd,  $J$  = 7.9, 1.5 Hz, 2H), 7.56–7.36 (m, 3H), 7.35–7.18 (m, 4H), 5.31 (s, 2H), 2.49 (s, 3H). <sup>13</sup>C NMR (101 MHz, CDCl<sub>3</sub>):  $\delta$  185.0, 154.2, 139.7, 133.6, 131.5, 131.1, 129.0, 128.9, 128.9, 128.7, 126.8, 121.3, 56.2, 15.5. MALDI-TOF *m/z*: calcd for C<sub>18</sub>H<sub>16</sub>N<sub>2</sub>O<sub>2</sub>S, 308.09; found, 308.24.

**3-Phenyl-1-(4-(trifluoromethoxy)benzyl)-1H-pyrazole-4-carbaldehyde (2d).** Compound **2d** was synthesized from 3-phenyl-1H-pyrazole-4-carbaldehyde (**1**), 4-(trifluoromethoxy)benzyl bromide (**d**) and potassium carbonate by following general procedure A (white solid, 90%). <sup>1</sup>H NMR (400 MHz, CDCl<sub>3</sub>):  $\delta$  9.96 (s, 1H), 8.03 (s, 1H), 7.75 (d,  $J$  = 7.1 Hz, 2H), 7.56–7.43 (m, 3H), 7.38 (d,  $J$  = 8.4 Hz, 2H), 7.26 (d,  $J$  = 8.2 Hz, 2H), 5.38 (s, 2H). <sup>13</sup>C NMR (101 MHz, CDCl<sub>3</sub>):  $\delta$  185.1, 154.4, 149.4, 133.6, 133.5, 131.4, 129.7, 129.2, 128.9, 128.8, 121.5, 121.4, 55.8. MALDI-TOF *m/z*: calcd for C<sub>18</sub>H<sub>13</sub>F<sub>3</sub>N<sub>2</sub>O<sub>2</sub>, 346.09; found, 346.18.

**3-Phenyl-1-(3-(trifluoromethoxy)benzyl)-1H-pyrazole-4-carbaldehyde (2e).** Compound **2e** was synthesized from 3-phenyl-1H-pyrazole-4-carbaldehyde (**1**), 3-(trifluoromethoxy)benzyl bromide (**e**) and potassium carbonate by following general procedure A (white semi solid, 91%). <sup>1</sup>H NMR (400 MHz, CDCl<sub>3</sub>):  $\delta$  9.95 (s, 1H), 8.01 (s, 1H), 7.73 (dd,  $J$  = 7.9, 1.6 Hz, 2H), 7.62–7.32 (m, 4H), 7.25–7.16 (m, 3H), 5.38 (s, 2H), 1.62 (s, 1H). <sup>13</sup>C NMR (101 MHz, CDCl<sub>3</sub>):  $\delta$  185.1, 154.5, 149.7, 137.1, 133.9, 131.4, 130.6, 129.2, 128.9, 128.8, 126.3, 121.6, 121.0, 120.6, 56.0. MALDI-TOF *m/z*: calcd for C<sub>18</sub>H<sub>13</sub>F<sub>3</sub>N<sub>2</sub>O<sub>2</sub>, 346.09; found, 346.17.

**1-Phenethyl-3-phenyl-1H-pyrazole-4-carbaldehyde (2f).** Compound **2f** was synthesized from 3-phenyl-1H-pyrazole-4-carbaldehyde (**1**), 2-phenylethyl bromide (**f**), and potassium carbonate by following general procedure A (colorless oil, 91%). <sup>1</sup>H NMR (400 MHz, CDCl<sub>3</sub>):  $\delta$  9.88 (s, 1H), 8.03–7.65 (m, 3H), 7.58–7.37 (m, 3H), 7.37–7.17 (m, 3H), 7.10 (d,  $J$  = 6.7 Hz, 2H), 4.40 (t,  $J$  = 7.2 Hz, 2H), 3.24 (t,  $J$  = 7.2 Hz, 2H). <sup>13</sup>C NMR (101 MHz, CDCl<sub>3</sub>):  $\delta$  185.0, 154.2, 137.2, 134.1, 131.7, 129.0, 128.9, 128.8, 128.7, 128.6, 127.0, 120.6, 54.3, 36.4. MALDI-TOF *m/z*: calcd for C<sub>18</sub>H<sub>16</sub>N<sub>2</sub>O, 276.13; found, 346.34.

**3-Phenyl-1-(2-(piperidin-1-yl)ethyl)-1H-pyrazole-4-carbaldehyde (2g).** Compound **2g** was synthesized from 3-phenyl-1H-pyrazole-4-carbaldehyde (**1**), 1-(2-chloroethyl)piperidine hydrochloride (**g**), and potassium carbonate by following general procedure A (colorless oil, 46%). <sup>1</sup>H NMR (400 MHz, CDCl<sub>3</sub>):  $\delta$  9.94 (s, 1H), 8.14 (s, 1H), 7.72 (dd,  $J$  = 8.0, 1.4 Hz, 2H), 7.58–7.33 (m, 3H), 4.28 (t,  $J$  = 6.5 Hz, 2H), 2.81 (t,  $J$  = 6.5 Hz, 2H), 2.65–2.33 (m, 4H), 1.58 (dt,  $J$  = 11.0, 5.6 Hz, 4H), 1.50–1.33 (m, 2H). <sup>13</sup>C NMR (101 MHz, CDCl<sub>3</sub>):  $\delta$  185.1, 153.8, 134.4, 131.7, 129.0, 128.9, 128.7, 120.8, 58.0, 54.6, 50.5, 26.0, 24.2. MALDI-TOF *m/z*: calcd for C<sub>17</sub>H<sub>21</sub>N<sub>3</sub>O, 283.16; found, 283.38.

**1-(2-Morpholinoethyl)-3-phenyl-1H-pyrazole-4-carbaldehyde (2h).** Compound **2h** was synthesized from 3-phenyl-1H-pyrazole-4-carbaldehyde (**1**), 4-(2-chloroethyl)morpholine hydrochloride (**h**) and potassium carbonate by following general procedure A (pale yellow oil, 42%). <sup>1</sup>H NMR (400 MHz, CDCl<sub>3</sub>):  $\delta$  9.95 (s, 1H), 8.13 (s, 1H), 7.72 (dd,  $J$  = 7.9, 1.5 Hz, 2H), 7.53–7.42 (m, 3H), 4.30 (t,  $J$  = 6.3 Hz, 2H), 3.77–3.65 (m, 4H), 2.88 (t,  $J$  = 6.3 Hz, 2H), 2.59–2.43 (m, 4H). <sup>13</sup>C NMR (101 MHz, CDCl<sub>3</sub>):  $\delta$  185.0, 153.8, 134.4, 131.6, 129.0, 128.8, 128.6, 120.9, 66.8, 57.6, 53.5, 50.0. MALDI-TOF *m/z*: calcd for C<sub>16</sub>H<sub>19</sub>N<sub>3</sub>O<sub>2</sub>, 285.14; found, 285.37.

**3-Phenyl-1-(4-phenylbutyl)-1H-pyrazole-4-carbaldehyde (2i).** Compound **2i** was synthesized from 3-phenyl-1H-pyrazole-4-carbaldehyde (**1**), 4-phenylbutyl bromide (**i**), and potassium carbonate by following general procedure A (colorless oil, 86%). <sup>1</sup>H NMR (400 MHz, CDCl<sub>3</sub>):  $\delta$  9.96 (s, 1H), 8.00 (s, 1H), 7.73 (dd,  $J$  = 7.7, 1.8 Hz, 2H), 7.53–7.40 (m, 3H), 7.34–7.27 (m, 3H), 7.25–7.15 (m, 3H), 4.21 (t,  $J$  = 7.1 Hz, 2H), 2.69 (t,  $J$  = 7.5 Hz, 2H), 1.99 (p,  $J$  = 7.4 Hz, 2H), 1.78–1.63 (m, 2H). <sup>13</sup>C NMR (101 MHz, CDCl<sub>3</sub>):  $\delta$  185.1, 154.0,

141.5, 133.4, 131.7, 129.0, 128.9, 128.7, 128.4, 126.0, 120.8, 52.8, 35.2, 29.4, 28.2. MALDI-TOF  $m/z$ : calcd for  $C_{20}H_{20}N_2O$ , 304.15; found, 304.32.

**3-Phenyl-1-(8-phenyloctyl)-1H-pyrazole-4-carbaldehyde (2j).** Compound **2j** was synthesized from 3-phenyl-1H-pyrazole-4-carbaldehyde (**1**), 8-phenyloctyl bromide (**j**), and potassium carbonate by following general procedure A (colorless oil, 87%).  $^1H$  NMR (400 MHz,  $CDCl_3$ ):  $\delta$  9.97 (s, 1H), 8.03 (s, 1H), 7.84–7.69 (m, 2H), 7.55–7.42 (m, 3H), 7.38–7.23 (m, 3H), 7.19 (d,  $J$  = 7.4 Hz, 3H), 4.19 (t,  $J$  = 7.2 Hz, 2H), 2.61 (t,  $J$  = 7.7 Hz, 2H), 2.11–1.85 (m, 2H), 1.83–1.45 (m, 3H), 1.45–1.14 (m, 9H).  $^{13}C$  NMR (101 MHz,  $CDCl_3$ ):  $\delta$  185.2, 154.1, 142.8, 133.5, 131.8, 129.0, 128.9, 128.7, 128.4, 128.3, 125.6, 120.8, 53.0, 36.0, 31.4, 29.9, 29.3, 29.2, 29.0, 26.5. MALDI-TOF  $m/z$ : calcd for  $C_{24}H_{28}N_2O$ , 360.22; found, 360.27.

**General Procedure B for the Synthesis of 3(a,b).** **1,3-Dipropylpyrimidine-2,4,6(1H,3H,5H)-trione (3a).** **6a** (220 mg, 1.5 mmol) was added to a stirred solution of malonic acid (150 mg, 1.5 mmol) in acetic acid (5 mL) and acetic anhydride (3 mL). The resultant solution was heated to 90 °C for 4 h and cooled to room temperature. Then, the reaction mixture was treated with water (20 mL) and extracted with ethyl acetate ( $3 \times 10$  mL). The combined organic extracts were washed with brine, dried over  $Na_2SO_4$ , and evaporated. The resultant residue was purified by silica gel column chromatography (hexane–ethyl acetate, 3:1) to afford **3a** as a white solid (160 mg, 51%).  $^1H$  NMR (400 MHz,  $CDCl_3$ ):  $\delta$  4.02–3.75 (m, 4H), 3.67 (s, 2H), 1.75–1.51 (m, 4H), 0.95 (t,  $J$  = 7.5 Hz, 6H).  $^{13}C$  NMR (101 MHz,  $CDCl_3$ ):  $\delta$  164.6, 151.4, 43.5, 39.7, 21.3, 11.2. MALDI-TOF  $m/z$ : calcd for  $C_{10}H_{16}N_2O_3$ , 212.11; found, 211.37.

**1,3-Diphenethylpyrimidine-2,4,6(1H,3H,5H)-trione (3b).** Compound **3b** was synthesized from **6b** and malonic acid using acetic acid and acetic anhydride by following general procedure B (white solid, 57%).  $^1H$  NMR (400 MHz,  $CDCl_3$ ):  $\delta$  7.44–7.12 (m, 10H), 4.11 (t,  $J$  = 7 Hz, 4H), 3.58 (s, 2H), 2.89 (t,  $J$  = 7.4 Hz, 1H).  $^{13}C$  NMR (101 MHz,  $CDCl_3$ ):  $\delta$  164.3, 152.0, 137.8, 129.0, 128.6, 126.8, 43.0, 39.5, 34.0.

**General Procedure C for the Synthesis of 4(a–o).** **5-((1,3-Diphenyl-1H-pyrazol-4-yl)methylene)pyrimidine-2,4,6(1H,3H,5H)-trione (4a).** Piperidine (10  $\mu$ L) was added to a solution of 1,3-diphenyl-1H-pyrazole-4-carboxaldehyde (0.36 g, 1.46 mmol) and barbituric acid (0.170 g, 1.32 mmol) in methanol (10 mL) and stirred for 16 h. The resultant yellow solid was filtered and washed with cold methanol ( $2 \times 5$  mL) and dried to yield a pure compound **4a** as a yellow solid (433 mg, 91%).  $^1H$  NMR (400 MHz,  $DMSO-d_6$ ):  $\delta$  11.35 (s, 1H), 11.33 (s, 1H), 9.81 (s, 1H), 8.19 (s, 1H), 7.94 (d,  $J$  = 8.0 Hz, 2H), 7.70–7.54 (m, 7H), 7.48 (t,  $J$  = 7.4 Hz, 1H).  $^{13}C$  NMR (101 MHz,  $DMSO-d_6$ ):  $\delta$  163.6, 162.7, 157.9, 150.3, 143.5, 138.6, 130.8, 129.9, 129.5, 129.4, 128.9, 128.1, 119.7, 115.2, 114.5. MALDI-TOF  $m/z$ : calcd for  $C_{20}H_{14}N_4O_3$ , 358.10; found, 358.71.

**5-((1,3-Diphenyl-1H-pyrazol-4-yl)methylene)-1,3-dimethylpyrimidine-2,4,6(1H,3H,5H)-trione (4b).** Compound **4b** was synthesized from 1,3-diphenyl-1H-pyrazole-4-carboxaldehyde and 1,3-dimethylbarbituric acid using piperidine by following general procedure C (yellow solid, 74%).  $^1H$  NMR (400 MHz,  $CDCl_3$ ):  $\delta$  9.91 (s, 1H), 8.63 (s, 1H), 7.93 (d,  $J$  = 8.0 Hz, 2H), 7.67 (d,  $J$  = 7.0 Hz, 2H), 7.61–7.49 (m, 5H), 7.43 (t,  $J$  = 7.3 Hz, 1H), 3.46 (s, 3H), 3.42 (s, 3H).  $^{13}C$  NMR (101 MHz,  $CDCl_3$ ):  $\delta$  162.9, 161.7, 159.6, 151.5, 148.0, 139.0, 135.1, 130.9, 129.8, 129.6, 129.5, 129.0, 128.1, 120.1, 116.1, 112.6, 28.9, 28.3. MALDI-TOF  $m/z$ : calcd for  $C_{22}H_{18}N_4O_3$ , 386.13; found, 386.14.

**5-((1,3-Diphenyl-1H-pyrazol-4-yl)methylene)-1,3-dipropylpyrimidine-2,4,6(1H,3H,5H)-trione (4c).** Compound **4c** was synthesized from 1,3-diphenyl-1H-pyrazole-4-carboxaldehyde and 1,3-dipropylbarbituric acid (**3a**) using piperidine by following general procedure C (pale yellow solid, 71%).  $^1H$  NMR (400 MHz,  $CDCl_3$ ):  $\delta$  9.91 (s, 1H), 8.63 (s, 1H), 8.01–7.84 (m, 2H), 7.67 (dd,  $J$  = 7.9, 1.5 Hz, 2H), 7.61–7.51 (m, 5H), 7.43 (t,  $J$  = 7.4 Hz, 1H), 7.28 (s, 1H), 4.12–3.84 (m, 4H), 1.90–1.59 (m, 4H), 1.13–0.83 (m, 6H).  $^{13}C$  NMR (101 MHz,  $DMSO-d_6$ ):  $\delta$  162.5, 161.5, 158.7, 151.1, 145.2, 139.0, 134.9, 131.2, 130.4, 130.0, 129.9, 129.4, 128.7, 120.3, 115.8, 114.5, 43.6, 43.0, 21.2, 11.7, 11.6. MALDI-TOF  $m/z$ : calcd for  $C_{26}H_{26}N_4O_3$ , 442.20; found, 442.11.

**5-((1,3-Diphenyl-1H-pyrazol-4-yl)methylene)-1,3-diphenethylpyrimidine-2,4,6(1H,3H,5H)-trione (4d).** Compound **4d** was synthesized from 1,3-diphenyl-1H-pyrazole-4-carboxaldehyde and **3b** using piperidine by following general procedure C (pale yellow solid, 81%).  $^1H$  NMR (400 MHz,  $CDCl_3$ ):  $\delta$  9.84 (s, 1H), 8.61 (s, 1H), 7.95 (d,  $J$  = 7.6 Hz, 2H), 7.68 (dd,  $J$  = 7.9, 1.6 Hz, 2H), 7.63–7.53 (m, 5H), 7.45 (t,  $J$  = 7.4 Hz, 1H), 7.38–7.29 (m, 8H), 7.27–7.20 (m, 2H), 4.34–4.12 (m, 4H), 3.05–2.83 (m, 4H).  $^{13}C$  NMR (101 MHz,  $DMSO-d_6$ ):  $\delta$  162.4, 161.3, 158.7, 150.7, 145.4, 139.0, 138.9, 134.9, 131.1, 130.4, 130.0, 129.5, 129.2, 129.1, 128.9, 128.9, 128.7, 126.8, 120.3, 115.7, 114.4, 43.3, 42.6, 33.9. MALDI-TOF  $m/z$ : calcd for  $C_{36}H_{30}N_4O_3$ , 566.23; found, 566.80.

**5-((1-Benzyl-3-phenyl-1H-pyrazol-4-yl)methylene)pyrimidine-2,4,6(1H,3H,5H)-trione (4e).** Compound **4e** was synthesized from **2b** and barbituric acid using piperidine by following general procedure C (pale yellow solid, 88%).  $^1H$  NMR (400 MHz,  $DMSO-d_6$ ):  $\delta$  11.20 (s, 2H), 9.41 (s, 1H), 8.14 (s, 1H), 7.68–7.47 (m, 3H), 7.43–7.29 (m, 2H), 5.56 (s, 1H).  $^{13}C$  NMR (101 MHz,  $DMSO-d_6$ ):  $\delta$  164.3, 163.2, 157.9, 150.6, 144.7, 138.6, 136.7, 131.6, 130.0, 129.5, 129.3, 129.2, 128.6, 128.5, 114.0, 113.3, 55.6. MALDI-TOF  $m/z$ : calcd for  $C_{21}H_{16}N_4O_3$ , 372.12; found, 372.16.

**5-((1-(4-(Methylthio)benzyl)-3-phenyl-1H-pyrazol-4-yl)methylene)pyrimidine-2,4,6(1H,3H,5H)-trione (4f).** Compound **4f** was synthesized from **2c** and barbituric acid using piperidine by following general procedure C (pale yellow solid, 85%).  $^1H$  NMR (400 MHz,  $DMSO-d_6$ ):  $\delta$  11.23 (m, 1H), 11.19 (m, 1H), 9.40 (s, 1H), 8.13 (s, 1H), 7.61–7.43 (m, 5H), 7.36 (d,  $J$  = 8.3 Hz, 2H), 7.28 (d,  $J$  = 8.3 Hz, 2H), 5.51 (s, 2H), 2.46 (s, 3H).  $^{13}C$  NMR (101 MHz,  $DMSO-d_6$ ):  $\delta$  164.3, 163.2, 157.9, 150.7, 144.8, 138.8, 138.5, 133.0, 132.6, 130.0, 129.5, 129.4, 129.3, 126.5, 114.0, 113.3, 55.5, 15.0. MALDI-TOF  $m/z$ : calcd for  $C_{22}H_{18}N_4O_3S$ , 418.11; found, 440.69 (M + Na)<sup>+</sup>.

**5-((3-Phenyl-1-(4-(trifluoromethoxy)benzyl)-1H-pyrazol-4-yl)methylene)pyrimidine-2,4,6(1H,3H,5H)-trione (4g).** Compound **4g** was synthesized from **2d** and barbituric acid using piperidine by following general procedure C (pale yellow solid, 40%).  $^1H$  NMR (400 MHz,  $DMSO-d_6$ ):  $\delta$  11.23 (s, 2H), 9.47 (s, 1H), 8.15 (s, 1H), 7.64–7.46 (m, 7H), 7.40 (d,  $J$  = 8.1 Hz, 2H), 5.62 (s, 2H).  $^{13}C$  NMR (101 MHz,  $DMSO-d_6$ ):  $\delta$  164.3, 163.2, 158.1, 150.7, 148.5, 148.4, 144.7, 138.9, 136.2, 131.6, 130.6, 130.0, 129.6, 129.3, 121.8, 114.1, 113.5, 55.0. MALDI-TOF  $m/z$ : calcd for  $C_{22}H_{15}F_3N_4O_4$ , 456.10; found, 455.99.

**5-((3-Phenyl-1-(3-(trifluoromethoxy)benzyl)-1H-pyrazol-4-yl)methylene)pyrimidine-2,4,6(1H,3H,5H)-trione (4h).** Compound **4h** was synthesized from **2e** and barbituric acid using piperidine by following general procedure C (pale yellow solid, 47%).  $^1H$  NMR (400 MHz,  $DMSO-d_6$ ):  $\delta$  11.23 (s, 2H), 9.48 (s, 1H), 8.14 (s, 1H), 7.60–7.47 (m, 6H), 7.45–7.32 (m, 3H), 5.65 (s, 2H).  $^{13}C$  NMR (101 MHz,  $DMSO-d_6$ ):  $\delta$  164.3, 163.2, 158.1, 150.7, 148.9, 144.6, 139.4, 139.0, 131.5, 131.3, 130.0, 129.6, 129.3, 127.6, 121.0, 114.0, 113.6, 55.0. MALDI-TOF  $m/z$ : calcd for  $C_{22}H_{15}F_3N_4O_4$ , 456.10; found, 456.67.

**5-((1-Phenethyl-3-phenyl-1H-pyrazol-4-yl)methylene)pyrimidine-2,4,6(1H,3H,5H)-trione (4i).** Compound **4i** was synthesized from **2f** and barbituric acid using piperidine by following general procedure C (pale yellow solid, 57%).  $^1H$  NMR (400 MHz,  $DMSO-d_6$ ):  $\delta$  11.18 (s, 2H), 9.24 (s, 1H), 8.12 (s, 1H), 7.65–7.44 (m, 5H), 7.38–7.15 (m, 5H), 4.57 (t,  $J$  = 7.3 Hz, 2H), 3.21 (t,  $J$  = 7.2 Hz, 2H).  $^{13}C$  NMR (101 MHz,  $DMSO-d_6$ ):  $\delta$  164.3, 163.1, 157.8, 150.7, 144.9, 138.7, 138.3, 131.7, 130.0, 129.5, 129.3, 129.2, 128.9, 127.0, 113.6, 112.9, 53.6, 36.0. MALDI-TOF  $m/z$ : calcd for  $C_{22}H_{18}N_4O_3$ , 386.13; found, 386.75.

**5-((3-Phenyl-1-(2-(piperidin-1-yl)ethyl)-1H-pyrazol-4-yl)methylene)pyrimidine-2,4,6(1H,3H,5H)-trione (4j).** Compound **4j** was synthesized from **2g** and barbituric acid using piperidine by following general procedure C (pale yellow solid, 66%).  $^1H$  NMR (400 MHz,  $DMSO-d_6$ ):  $\delta$  11.19 (s, 2H), 9.38 (s, 1H), 8.16 (s, 1H), 7.64–7.44 (m, 5H), 4.40 (t,  $J$  = 6.2 Hz, 2H), 2.74 (t,  $J$  = 6.3 Hz, 2H), 2.46–2.25 (m, 4H), 1.56–1.42 (m, 4H), 1.44–1.25 (m, 2H).  $^{13}C$  NMR (100 MHz,  $DMSO-d_6$ ):  $\delta$  164.4, 163.2, 157.5, 150.7, 145.0, 139.1, 131.8, 130.0, 129.4, 129.3, 113.7, 112.8, 58.0, 54.3, 50.2, 26.0, 24.2. MALDI-TOF  $m/z$ : calcd for  $C_{21}H_{23}N_5O_3$ , 393.18; found, 391.78.

5-((1-(2-Morpholinoethyl)-3-phenyl-1H-pyrazol-4-yl)methylene)pyrimidine-2,4,6(1H,3H,5H)-trione (**4k**). Compound **4k** was synthesized from **2h** and barbituric acid using piperidine by following general procedure C (yellow solid, 69%). <sup>1</sup>H NMR (400 MHz, DMSO-*d*<sub>6</sub>): δ 11.28–11.07 (m, 2H), 9.41 (s, 1H), 8.16 (s, 1H), 7.64–7.45 (m, 5H), 4.44 (t, *J* = 6.1 Hz, 2H), 3.63–3.49 (m, 4H), 2.79 (t, *J* = 5.9 Hz, 2H), 2.49–2.41 (m, 4H). <sup>13</sup>C NMR (101 MHz, DMSO-*d*<sub>6</sub>): δ 164.4, 163.2, 157.4, 150.7, 145.0, 139.2, 131.7, 130.0, 129.5, 129.3, 113.7, 112.9, 66.6, 57.5, 53.5, 49.7. MALDI-TOF *m/z*: calcd for C<sub>20</sub>H<sub>21</sub>N<sub>5</sub>O<sub>4</sub>, 395.15; found, 395.77.

5-((3-Phenyl-1-(4-phenylbutyl)-1H-pyrazol-4-yl)methylene)pyrimidine-2,4,6(1H,3H,5H)-trione (**4l**). Compound **4l** was synthesized from **2i** and barbituric acid using piperidine by following general procedure C (pale yellow solid, 80%). <sup>1</sup>H NMR (300 MHz, DMSO-*d*<sub>6</sub>): δ 11.18 (s, 2H), 9.33 (s, 1H), 8.15 (s, 1H), 7.62–7.38 (m, 5H), 7.32–7.22 (m, 2H), 7.22–7.12 (m, 3H), 4.34 (t, *J* = 6.9 Hz, 2H), 2.63 (t, *J* = 7.6 Hz, 2H), 1.99–1.75 (m, 2H), 1.69–1.46 (m, 2H). <sup>13</sup>C NMR (100 MHz, DMSO-*d*<sub>6</sub>): δ 164.3, 163.2, 157.7, 150.8, 145.0, 142.2, 138.5, 131.8, 129.9, 129.5, 129.3, 128.8, 128.7, 126.2, 113.6, 113.0, 52.3, 34.9, 29.5, 28.2. MALDI-TOF *m/z*: calcd for C<sub>24</sub>H<sub>22</sub>N<sub>4</sub>O<sub>3</sub>, 414.16; found, 414.77.

5-((3-Phenyl-1-(8-phenyloctyl)-1H-pyrazol-4-yl)methylene)pyrimidine-2,4,6(1H,3H,5H)-trione (**4m**). Compound **4m** was synthesized from **2j** and barbituric acid using piperidine by following general procedure C (white solid, 80%). <sup>1</sup>H NMR (300 MHz, DMSO-*d*<sub>6</sub>): δ 11.20 (s, 2H), 9.32 (s, 1H), 8.15 (s, 1H), 7.60–7.41 (m, 5H), 7.29–7.21 (m, 2H), 7.20–7.08 (m, 3H), 4.30 (t, *J* = 6.9 Hz, 2H), 2.65–2.52 (m, 2H), 1.97–1.70 (m, 2H), 1.66–1.41 (m, 2H), 1.39–1.10 (m, 8H). <sup>13</sup>C NMR (101 MHz, DMSO-*d*<sub>6</sub>): δ 164.4, 163.2, 157.6, 150.8, 144.9, 142.7, 138.4, 131.8, 129.9, 129.4, 129.2, 128.9, 128.6, 126.0, 113.7, 112.9, 52.5, 35.6, 31.4, 29.8, 29.1, 29.0, 28.8, 26.3. MALDI-TOF *m/z*: calcd for C<sub>28</sub>H<sub>30</sub>N<sub>4</sub>O<sub>3</sub>, 470.23; found, 470.79.

1,3-Dimethyl-5-((3-phenyl-1-(4-phenylbutyl)-1H-pyrazol-4-yl)methylene)pyrimidine-2,4,6(1H,3H,5H)-trione (**4n**). Compound **4n** was synthesized from **2i** and 1,3-dimethylbarbituric acid using piperidine by following general procedure C (white solid, 87%). <sup>1</sup>H NMR (400 MHz, CDCl<sub>3</sub>): δ 9.36 (s, 1H), 8.58 (s, 1H), 7.62–7.44 (m, 5H), 7.39–7.26 (m, 2H), 7.21 (t, *J* = 8.7 Hz, 3H), 4.28 (t, *J* = 7.2 Hz, 2H), 3.44 (s, 3H), 3.40 (s, 3H), 2.71 (t, *J* = 7.6 Hz, 2H), 2.16–1.98 (m, 2H), 1.82–1.64 (m, 2H). <sup>13</sup>C NMR (101 MHz, CDCl<sub>3</sub>): δ 163.1, 161.8, 159.1, 151.5, 148.7, 141.6, 138.2, 131.1, 129.7, 129.3, 128.9, 128.4, 128.4, 126.0, 114.4, 111.4, 53.0, 35.3, 29.6, 28.9, 28.3, 28.2. MALDI-TOF *m/z*: calcd for C<sub>26</sub>H<sub>26</sub>N<sub>4</sub>O<sub>3</sub>, 442.20; found, 442.78.

1,3-Dimethyl-5-((3-phenyl-1-(8-phenyloctyl)-1H-pyrazol-4-yl)methylene)pyrimidine-2,4,6(1H,3H,5H)-trione (**4o**). Compound **4o** was synthesized from **2j** and 1,3-dimethylbarbituric acid using piperidine by following general procedure C (white solid, 89%). <sup>1</sup>H NMR (400 MHz, CDCl<sub>3</sub>): δ 9.26 (s, 1H), 8.49 (s, 1H), 7.55–7.33 (m, 5H), 7.18 (t, *J* = 7.5 Hz, 2H), 7.08 (d, *J* = 7.6 Hz, 3H), 4.22–4.09 (m, 2H), 3.33 (s, 3H), 3.29 (s, 3H), 2.51 (t, *J* = 7.7 Hz, 2H), 2.02–1.78 (m, 2H), 1.61–1.43 (m, 2H), 1.35–1.20 (m, 8H). <sup>13</sup>C NMR (101 MHz, CDCl<sub>3</sub>): δ 163.1, 161.6, 159.1, 151.5, 148.8, 142.8, 138.1, 131.2, 129.7, 129.2, 128.9, 128.4, 128.3, 125.6, 114.4, 111.3, 53.2, 35.9, 31.4, 30.0, 29.3, 29.2, 29.0, 28.8, 28.2, 26.6. MALDI-TOF *m/z*: calcd for C<sub>30</sub>H<sub>34</sub>N<sub>4</sub>O<sub>3</sub>, 498.26; found, 498.81.

**General Procedure D for the Synthesis of 6(a,b).** 1,3-Dipropylurea (**6a**). To a stirred solution of *S,S'*-dimethyl dithiocarbamate (1.17 g, 5 mmol) in methanol (10 mL), propylamine (0.719 g, 10.5 mmol) was added and heated to 60 °C for 24 h. The reaction mixture was evaporated under vacuum, and the resultant crude mixture was treated with diethyl ether and hexane to obtain the product **6a** (308 mg, 43%) as a white solid. <sup>1</sup>H NMR (400 MHz, CDCl<sub>3</sub>): δ 4.48 (s, 2H), 3.14 (q, *J* = 7.4 Hz, 4H), 1.53 (p, *J* = 7.4 Hz, 4H), 0.94 (t, *J* = 7.4 Hz, 6H). <sup>13</sup>C NMR (101 MHz, CDCl<sub>3</sub>): δ 158.9, 42.2, 23.6, 11.4.

1,3-Diphenethylurea (**6b**). Compound **6b** was synthesized by following general procedure D using *S,S'*-dimethyl dithiocarbamate and phenylethylamine (white solid, 69%). <sup>1</sup>H NMR (400 MHz, CDCl<sub>3</sub>): δ 7.40–7.10 (m, 10H), 4.19 (s, 2H), 3.42 (q, *J* = 6.7 Hz, 4H), 2.79 (t, *J* = 6.8 Hz, 4H). <sup>13</sup>C NMR (101 MHz, CDCl<sub>3</sub>): δ 158.2, 139.2, 128.8,

128.5, 126.4, 41.6, 36.5. MALDI-TOF *m/z*: calcd for C<sub>17</sub>H<sub>20</sub>N<sub>2</sub>O, 268.15; found, 268.38.

*tert*-Butyl(2-(4-formyl-3-phenyl-1H-pyrazol-1-yl)ethyl)carbamate (**7**). Compound **7** was synthesized from 3-phenyl-1H-pyrazole-4-carbaldehyde (**1**), 2-(Boc-amino)ethyl bromide, and potassium carbonate by following general procedure A (white solid, 70%). <sup>1</sup>H NMR (500 MHz, CDCl<sub>3</sub>): δ 9.98 (s, 1H), 8.04 (s, 1H), 7.75 (d, *J* = 6.8 Hz, 2H), 7.56–7.41 (m, 3H), 4.87 (s, 1H), 4.34 (s, 2H), 3.75–3.58 (m, 2H), 1.47 (s, 9H). <sup>13</sup>C NMR (101 MHz, CDCl<sub>3</sub>): δ 185.2, 154.6, 150.3, 138.4, 134.8, 131.4, 130.1, 129.1, 128.8, 120.9, 120.3, 80.2, 52.4, 40.4, 28.3.

1-(2-Aminoethyl)-3-phenyl-1H-pyrazole-4-carbaldehyde Hydrochloride (**8**). 2 M HCl (11 mL, 22 mmol) in diethyl ether was added to the stirred solution of **7** (700 mg, 2.22 mmol) in 10 mL of dichloromethane. The resultant solution was stirred for 16 h at room temperature, and the solid formed was filtered and washed with anhydrous diethyl ether to yield **8** as a pale yellow solid (537 mg, 96%). <sup>1</sup>H NMR (400 MHz, DMSO-*d*<sub>6</sub>): δ 9.89 (s, 1H), 8.66 (s, 1H), 8.64–8.36 (m, 3H), 7.90–7.79 (m, 2H), 7.51–7.34 (m, 3H), 4.58 (d, *J* = 6.1 Hz, 2H), 3.34 (q, *J* = 5.8 Hz, 2H). <sup>13</sup>C NMR (101 MHz, DMSO-*d*<sub>6</sub>): δ 185.0, 152.6, 138.7, 132.1, 129.3, 129.1, 128.9, 121.0, 49.5, 38.7. MALDI-TOF *m/z*: calcd for C<sub>12</sub>H<sub>13</sub>N<sub>3</sub>O, 215.10; found, 215.44.

**General Procedure E for the Synthesis of 9(a–d).** *N*-(2-(4-Formyl-3-phenyl-1H-pyrazol-1-yl)ethyl)cyclohexanecarboxamide (**9a**). To a stirred solution of EDCI (607 mg, 3.18 mmol), HOBt (428 mg, 3.18 mmol) in DMF (10 mL), cyclohexanecarboxylic acid (406 mg, 3.18 mmol), and DIEA (2.76 mL, 15.86 mmol) were added and stirred for 30 min. To the resultant solution, **8** (957 mg, 3.82 mmol) in DMF (5 mL) was added and it was stirred at room temperature for 18 h. The reaction mixture was treated with 5% NaHCO<sub>3</sub> solution (20 mL) and extracted with ethyl acetate (2 × 15 mL); the combined organic layer was washed with H<sub>2</sub>O and brine, dried over Na<sub>2</sub>SO<sub>4</sub>, and evaporated under vacuum. The crude residue was purified by flash column chromatography [CH<sub>2</sub>Cl<sub>2</sub>/ethyl acetate (3:1)] to provide **9a** (0.34 g, 43%) as a yellow solid. <sup>1</sup>H NMR (400 MHz, CDCl<sub>3</sub>): δ 9.95 (s, 1H), 7.98 (s, 1H), 7.74 (dd, *J* = 7.8, 1.6 Hz, 2H), 7.56–7.39 (m, 3H), 6.00 (s, 1H), 4.41–4.21 (m, 2H), 3.75 (q, *J* = 5.7 Hz, 2H), 2.15–1.98 (m, 1H), 1.90–1.70 (m, 4H), 1.69–1.58 (m, 1H), 1.51–1.32 (m, 2H), 1.33–1.08 (m, 3H). <sup>13</sup>C NMR (101 MHz, CDCl<sub>3</sub>): δ 184.8, 176.7, 154.5, 134.9, 131.7, 129.2, 128.8, 128.7, 120.9, 51.9, 45.3, 39.3, 29.6, 25.7, 25.6. MALDI-TOF *m/z*: calcd for C<sub>19</sub>H<sub>23</sub>N<sub>3</sub>O<sub>2</sub>, 325.17; found, 325.81.

*N*-(2-(4-Formyl-3-phenyl-1H-pyrazol-1-yl)ethyl)benzamide (**9b**). Compound **9b** was synthesized by following general procedure E using benzoic acid and amine salt **8** in the presence of EDCI, HOBt, and DIEA (white solid, 58%). <sup>1</sup>H NMR (400 MHz, CDCl<sub>3</sub>): δ 9.86 (s, 1H), 7.95 (s, 1H), 7.79–7.73 (m, 2H), 7.70 (dd, *J* = 6.5, 3.1 Hz, 2H), 7.52–7.42 (m, 4H), 7.41–7.33 (m, 2H), 7.33–7.24 (m, 1H), 4.46–4.32 (m, 2H), 3.92 (q, *J* = 5.6 Hz, 2H). <sup>13</sup>C NMR (101 MHz, CDCl<sub>3</sub>): δ 184.8, 167.8, 154.5, 135.1, 133.9, 131.8, 131.4, 129.2, 128.8, 128.7, 128.6, 127.0, 120.9, 51.8, 40.0. MALDI-TOF *m/z*: calcd for C<sub>19</sub>H<sub>17</sub>N<sub>3</sub>O<sub>2</sub>, 319.13; found, 319.78.

*N*-(2-(4-Formyl-3-phenyl-1H-pyrazol-1-yl)ethyl)-4-(methylsulfonyl)benzamide (**9c**). Compound **9c** was synthesized by following general procedure E using 4-(methylsulfonyl)benzoic acid and amine salt **8** in the presence of EDCI, HOBt, and DIEA (white solid, 65%). <sup>1</sup>H NMR (400 MHz, CDCl<sub>3</sub>): δ 10.00–9.86 (m, 1H), 8.04 (s, 1H), 8.01–7.84 (m, 4H), 7.71 (dd, *J* = 6.5, 3.1 Hz, 2H), 7.55–7.43 (m, 3H), 7.37 (t, *J* = 5.1 Hz, 1H), 4.53–4.38 (m, 2H), 3.99 (q, *J* = 5.5 Hz, 2H), 3.05 (s, 3H). <sup>13</sup>C NMR (101 MHz, DMSO-*d*<sub>6</sub>): δ 185.0, 165.9, 152.2, 143.5, 139.1, 138.2, 132.2, 129.2, 128.9, 128.9, 128.7, 127.5, 120.8, 51.6, 43.7. MALDI-TOF *m/z*: calcd for C<sub>20</sub>H<sub>19</sub>N<sub>3</sub>O<sub>4</sub>S, 397.10; found, 397.74.

*N*-(2-(4-Formyl-3-phenyl-1H-pyrazol-1-yl)ethyl)-4-(methylamino)benzamide (**9d**). Compound **9d** was synthesized by following general procedure E using 4-(methylamino)benzoic acid and amine salt **8** in the presence of EDCI, HOBt, and DIEA (semisolid, 55%). <sup>1</sup>H NMR (400 MHz, CDCl<sub>3</sub>): δ 9.89 (s, 1H), 7.96 (s, 1H), 7.74 (dd, *J* = 7.6, 1.8 Hz, 2H), 7.60 (d, *J* = 8.7 Hz, 2H), 7.52–7.39 (m, 3H), 6.80 (t, *J* = 5.2 Hz, 1H), 6.52 (d, *J* = 8.7 Hz, 2H), 4.47–4.33 (m, 2H), 4.17 (s, 1H), 3.90 (q, *J* = 5.6 Hz, 2H), 2.85 (s, 3H). <sup>13</sup>C NMR (101

MHz, CDCl<sub>3</sub>):  $\delta$  184.8, 167.7, 154.3, 152.1, 135.2, 131.5, 129.1, 128.8, 128.7, 121.7, 120.9, 111.4, 52.1, 39.9, 30.2 (traces of dichloromethane are present). MALDI-TOF  $m/z$ : calcd for C<sub>20</sub>H<sub>20</sub>N<sub>4</sub>O<sub>2</sub>, 348.15; found, 348.77, 360.76 (M + Na)<sup>+</sup>.

**General Procedure F for the Synthesis of 10(a–d).** *N*-(2-(3-Phenyl-4-((2,4,6-trioxotetrahydropyrimidin-5(2H)-ylidene)methyl)-1H-pyrazol-1-yl)ethyl)cyclohexanecarboxamide (**10a**). Barbituric acid (0.269 g, 2.1 mmol) was added to a stirred solution of **9a** (760 mg, 2.3 mmol) in dry methanol (15 mL) and heated to reflux for 16 h. The resultant yellow solid was filtered and washed with cold methanol (3 × 5 mL) and dried to yield pure compound **10a** as a yellow solid (776 mg, 84%). <sup>1</sup>H NMR (400 MHz, DMSO-*d*<sub>6</sub>):  $\delta$  11.21 (s, 2H), 9.27 (s, 1H), 8.16 (s, 1H), 7.86 (t, *J* = 5.6 Hz, 1H), 7.64–7.43 (m, 5H), 4.34 (t, *J* = 5.6 Hz, 2H), 3.50 (d, *J* = 5.6 Hz, 2H), 2.10–1.93 (m, 1H), 1.73–1.51 (m, 5H), 1.37–0.99 (m, 5H). <sup>13</sup>C NMR (101 MHz, DMSO-*d*<sub>6</sub>):  $\delta$  176.0, 164.3, 163.2, 157.9, 150.7, 145.0, 139.1, 131.8, 130.0, 129.5, 129.3, 113.8, 112.8, 52.0, 44.3, 39.0, 29.6, 25.9, 25.7. MALDI-TOF  $m/z$ : calcd for C<sub>23</sub>H<sub>25</sub>N<sub>5</sub>O<sub>4</sub>, 435.19; found, 435.76, 457.75 (M + Na)<sup>+</sup>.

*N*-(2-(3-Phenyl-4-((2,4,6-trioxotetrahydropyrimidin-5(2H)-ylidene)methyl)-1H-pyrazol-1-yl)ethyl)benzamide (**10b**). Compound **10b** was synthesized from **9b** and barbituric acid by following general procedure F (pale yellow solid, 68%). <sup>1</sup>H NMR (400 MHz, DMSO-*d*<sub>6</sub>):  $\delta$  11.20 (s, 2H), 9.35 (s, 1H), 8.66 (t, *J* = 5.4 Hz, 1H), 8.15 (s, 1H), 7.80 (d, *J* = 7.2 Hz, 2H), 7.65–7.36 (m, 8H), 4.51 (t, *J* = 5.6 Hz, 2H), 3.75 (q, *J* = 5.4 Hz, 2H). <sup>13</sup>C NMR (101 MHz, DMSO-*d*<sub>6</sub>):  $\delta$  167.3, 164.3, 163.2, 157.8, 150.7, 144.9, 139.1, 134.8, 131.7, 131.7, 129.9, 129.5, 129.2, 128.8, 127.7, 113.8, 112.9, 51.9, 39.9. MALDI-TOF  $m/z$ : calcd for C<sub>23</sub>H<sub>19</sub>N<sub>5</sub>O<sub>4</sub>, 429.14; found, 451.68 (M + Na)<sup>+</sup>.

4-(Methylsulfonyl)-*N*-(2-(3-phenyl-4-((2,4,6-trioxotetrahydropyrimidin-5(2H)-ylidene)methyl)-1H-pyrazol-1-yl)ethyl)benzamide (**10c**). Compound **10c** was synthesized from **9c** and barbituric acid by following general procedure F (yellow solid, 81%). <sup>1</sup>H NMR (400 MHz, DMSO-*d*<sub>6</sub>):  $\delta$  11.30–11.08 (m, 2H), 9.36 (s, 1H), 8.93 (t, *J* = 5.4 Hz, 1H), 8.14 (s, 1H), 8.09–7.94 (m, 4H), 7.61–7.38 (m, 5H), 4.53 (t, *J* = 5.5 Hz, 2H), 3.77 (q, *J* = 5.3 Hz, 2H), 3.26 (s, 3H). <sup>13</sup>C NMR (101 MHz, DMSO-*d*<sub>6</sub>):  $\delta$  166.1, 164.3, 163.2, 157.8, 150.6, 144.9, 143.4, 139.3, 139.1, 131.7, 129.9, 129.5, 129.3, 128.7, 127.5, 113.9, 113.0, 51.8, 43.8. MALDI-TOF  $m/z$ : calcd for C<sub>24</sub>H<sub>21</sub>N<sub>5</sub>O<sub>6</sub>S, 507.12; found, 507.68.

4-(Methylamino)-*N*-(2-(3-phenyl-4-((2,4,6-trioxotetrahydropyrimidin-5(2H)-ylidene)methyl)-1H-pyrazol-1-yl)ethyl)benzamide or KBJK557 (**10d**). Compound **10d** was synthesized from **9d** and barbituric acid by following general procedure F (yellow solid, 83%). <sup>1</sup>H NMR (400 MHz, DMSO-*d*<sub>6</sub>):  $\delta$  11.19 (s, 2H), 9.32 (s, 1H), 8.23 (t, *J* = 5.4 Hz, 1H), 8.15 (s, 1H), 7.70–7.40 (m, 7H), 6.51 (d, *J* = 8.7 Hz, 2H), 6.19 (q, *J* = 4.7 Hz, 1H), 4.47 (t, *J* = 5.8 Hz, 2H), 3.70 (q, *J* = 5.8 Hz, 2H), 2.71 (d, *J* = 4.9 Hz, 3H). <sup>13</sup>C NMR (101 MHz, DMSO-*d*<sub>6</sub>):  $\delta$  167.2, 164.3, 163.2, 157.8, 152.7, 150.7, 144.9, 139.0, 131.7, 130.0, 129.5, 129.2, 129.2, 121.1, 113.8, 112.9, 110.8, 52.2, 39.9, 29.8. MALDI-TOF  $m/z$ : calcd for C<sub>24</sub>H<sub>22</sub>N<sub>6</sub>O<sub>4</sub>, 458.17; found, 458.74.

(9H-Fluoren-9-yl)methyl 4-((2-(3-phenyl-4-((2,4,6-trioxotetrahydropyrimidin-5(2H)-ylidene)methyl)-1H-pyrazol-1-yl)ethyl)carbamoyl)benzylcarbamate (**11**). To a stirred solution of EDCI (607 mg, 3.18 mmol), HOBt (428 mg, 3.18 mmol) in DMF (10 mL), 4-(Fmoc-aminomethyl)benzoic acid (1.1 g, 3.18 mmol), and DIEA (2.76 mL, 15.86 mmol) were added and stirred for 30 min. To the resultant solution, **8** (957 mg, 3.82 mmol) in DMF (5 mL) was added and it was stirred at room temperature for 18 h. The reaction mixture was treated with 5% NaHCO<sub>3</sub> solution (25 mL) and extracted with ethyl acetate (3 × 15 mL); the combined organic layer was washed with H<sub>2</sub>O (3 × 20 mL) and brine, dried over Na<sub>2</sub>SO<sub>4</sub>, and evaporated under vacuum. To the crude product in methanol (15 mL), barbituric acid (0.269 g, 3.10 mmol) was added and heated to reflux for 16 h. The resultant yellow solid was filtered and washed with cold methanol (3 × 5 mL) and dried to yield pure compound **11** as a yellow solid (1.08 g, 50%). <sup>1</sup>H NMR (400 MHz, DMSO-*d*<sub>6</sub>):  $\delta$  11.24 (s, 1H), 11.21 (s, 1H), 9.35 (s, 1H), 8.65 (s, 1H), 8.16 (s, 1H), 7.89 (d, *J* = 5.6 Hz, 3H), 7.76 (d, *J* = 6.6 Hz, 2H), 7.71 (d, *J* = 6.4 Hz, 2H), 7.59–7.47 (m, 5H), 7.47–7.37 (m, 2H), 7.37–7.31 (m, 2H), 7.28 (d, *J* = 6.7 Hz, 2H), 4.58–4.45 (m, 2H), 4.44–4.32 (m, 2H), 4.30–4.16 (m, 3H), 3.85–3.67 (m, 2H). <sup>13</sup>C NMR (101 MHz, DMSO-*d*<sub>6</sub>):  $\delta$  167.0, 164.3, 163.2, 157.7, 156.9, 150.7,

144.9, 144.3, 143.6, 141.2, 139.1, 133.3, 131.7, 130.1, 129.5, 129.3, 128.1, 127.7, 127.5, 127.2, 125.6, 120.6, 113.9, 113.0, 65.8, 51.9, 47.3, 44.0. MALDI-TOF  $m/z$ : calcd for C<sub>39</sub>H<sub>32</sub>N<sub>6</sub>O<sub>6</sub>, 680.23; found, 703.2 (M + Na)<sup>+</sup>.

**Synthesis of 12.** 4-(Aminomethyl)-*N*-(2-(3-phenyl-4-((2,4,6-trioxotetrahydropyrimidin-5(2H)-ylidene)methyl)-1H-pyrazol-1-yl)ethyl)benzamide (**12**). To the stirred solution of **11** (150 mg, 0.222 mmol) in DMF (1.4 mL), piperidine (0.6 mL) was added dropwise and stirred for 3 h. The solid formed was filtered; the filtrate was treated with diethylether (30 mL) and the precipitated solids were filtered and dried to yield **12** as a white solid (101 mg, 53%). <sup>1</sup>H NMR (500 MHz, DMSO-*d*<sub>6</sub>):  $\delta$  8.52 (t, *J* = 4.8 Hz, 1H), 8.46 (s, 1H), 8.05 (s, 1H), 7.75 (d, *J* = 7.5 Hz, 2H), 7.66 (d, *J* = 7.5 Hz, 2H), 7.49 (t, *J* = 7.3 Hz, 2H), 7.42 (t, *J* = 7.2 Hz, 1H), 7.35 (d, *J* = 7.7 Hz, 2H), 4.68 (s, 2H), 4.42 (s, 2H), 3.70 (s, 2H) (traces of diethyl ether is present). <sup>13</sup>C NMR (101 MHz, DMSO-*d*<sub>6</sub>):  $\delta$  166.9, 154.9, 151.4, 143.9, 133.2, 133.1, 132.1, 129.1, 128.9, 128.8, 128.5, 128.3, 127.7, 117.3, 64.6, 51.7. MALDI-TOF  $m/z$ : calcd for C<sub>24</sub>H<sub>23</sub>N<sub>6</sub>O<sub>4</sub>, 458.17; found, 459.13, 481.11 (M + Na)<sup>+</sup>.

3,3-Dimethyl-1-(6-oxo-6-((4-((2-(3-phenyl-4-((2,4,6-trioxotetrahydropyrimidin-5(2H)-ylidene)methyl)-1H-pyrazol-1-yl)ethyl)carbamoyl)benzylamino)hexyl)-2-((1E,3E,5E)-5-(1,3,3-trimethylindolin-2-ylidene)penta-1,3-dien-1-yl)-3H-indol-1-ium Chloride (**14**). To the stirred solution of **12** (5.2 mg, 0.0109 mmol) in 1.5 mL of DMF, cyanine-5 NH ester (0.008116 mmol) was added and stirred for 16 h under dark reaction conditions at room temperature. Purification of the crude compound was carried out on the preparative Vydac C<sub>18</sub> column using a 10–90% water/acetonitrile gradient in the presence of 0.05% TFA for 30 min (A: water buffer, B: acetonitrile buffer). The purified compound (>95%) was assessed by RP HPLC on an analytical Vydac C<sub>18</sub> column. MALDI-TOF  $m/z$ : calcd for C<sub>56</sub>H<sub>59</sub>N<sub>8</sub>O<sub>5</sub>, 923.42; found, 923.52.

**Structure-Based High-Throughput Virtual Screening.** Structure-based virtual screening was carried out using the DOCK6.9 program ([http://dock.compbio.ucsf.edu/DOCK\\_6/index.htm](http://dock.compbio.ucsf.edu/DOCK_6/index.htm)).<sup>37</sup> In this analysis, we confirmed that relocation of ligands is possible using an X-ray crystal structure (3RQ7) containing a peptide-based inhibitor.<sup>20</sup> Among the two algorithms, namely, anchor and grow (flexible) and rigid of DOCK6.9, a rigid algorithm was confirmed as a suitable one for further analyses. The docking was performed using the MLSMR database. Structurally analogous compounds were searched using the ZINC database,<sup>38</sup> and approximately 20,000 compounds were docked. Finally, we identified **4a** as a hit compound.

**PBD FP Binding Assays for Plk1, Plk2, and Plk3.** FP assays were carried out essentially as described previously.<sup>39</sup> Briefly, an appropriate 5-carboxyfluorescein-labeled PBD-binding peptide for Plk1, Plk2, or Plk3 was incubated at a final concentration of 2 nM with various concentrations of the bacterially expressed and purified PBD of Plk1, Plk2, or Plk3, respectively, in a binding buffer containing 10 mM Tris (pH 8.0), 1 mM EDTA, 50 mM NaCl, and 0.01% Nonidet P-40. FP was analyzed 10 min after mixing of all components in a 384-well format using a Molecular Devices SpectraMax Paradigm Multi-Mode Microplate Detection Platform. All experiments were performed in triplicate. Obtained data were plotted using GraphPad Prism software version 6.

**Pan Assay Interference Compounds.** As described above, FP assays were carried out with 65 nM of bacterially expressed Plk1 PBD and 5 nM of an FITC-labeled PBD-binding peptide in the presence of increasing concentrations of KBJK557 and L-cysteine at various concentrations (0, 0.78, and 1.95  $\mu$ M, respectively). mP values were determined 30 min after incubation. Data were plotted using GraphPad Prism software. This experiment was performed in triplicate.

**Immunofluorescence Staining.** For immunofluorescence observation, HeLa cells were seeded on 24-well microplates at 2 or 4 × 10<sup>4</sup> cells/mL and cultured for 24 h. The cells were further cultured with DMSO, nocodazole (200 nM), BI2536 (200 nM), and KBJK557 (200  $\mu$ M) for 18 h. The medium in the microplate wells was then removed and cells were fixed with 4% formaldehyde in PBS for 15 min and then permeabilized for 5 min with 0.1% NP-40 in PBS. The cells were washed with PBS containing 1% bovine serum albumin (PBS-1% BSA) and then treated with 5% bovine serum albumin for 20 min. The cells in each well were treated with anti-Plk1 (mouse) and anti-CREST

(human) antibody in PBS-0.1% BSA and then placed in a humidified atmosphere at room temperature and incubated for 1.5 h. After being washed with PBS-0.1% BSA, treated wells were incubated with Alexa Fluor 488-conjugated human anti-IgG antibody and Texas Red-conjugated mouse anti-IgG antibody in PBS-0.1% BSA and then incubated at room temperature for 60 min. After being washed with PBS-0.1% BSA, the dish wells were overlaid with DAPI for 10 min at room temperature and then washed with PBS-0.1% BSA. Fluorescence was photographed with an inverted Zeiss 710 confocal microscope (Carl Zeiss, Oberkochen, Germany). The signal intensity was measured by the ZEN2010 program (Carl Zeiss, Oberkochen, Germany).

**Cell Cycle Arrest Study by a Fluorescence-Activated Cell Sorter.** HeLa cells were seeded into  $4 \times 10^5$  cells in six-well plates and treated with BI2536 (100 nM) and KBJK557 (200  $\mu$ M) for 24 h. Cells were washed with PBS three times and fixed using 70% cold ethanol during vortexing. The fixed cells were stained with propidium iodide (PI) (1  $\mu$ g/mL, Sigma-Aldrich, USA) and treated with RNase (1  $\mu$ g/mL) (Thermo Scientific, USA) in PBS for 30 min at 37 °C in an incubator. Flow cytometric analysis was performed using a fluorescence-activated cell sorter (Beckman Coulter, CytoFLEX, USA).

**Apoptosis.** HeLa cells ( $1 \times 10^4$  cells) were cultured in 96-well microplates for 24 h at 37 °C. Cells were treated with BI2536 (100 nM) and KBJK557 (200  $\mu$ M) at 24 and 48 h. Then, 2.5  $\mu$ L of mixtures of kit (LIVE/DEAD Viability/Cytotoxicity Kit, Invitrogen, USA) was added to 1 mL of PBS, and 100  $\mu$ L of this solution was added to each well. After 30 min of incubation at room temperature, images of the cells were captured by a fluorescence microscope (Nikon ECLIPSE TS100, Japan). The cell count was measured using ImageJ software.

**Cellular Uptake of a Fluorescence-Conjugated Inhibitor.** Cy5 NHS ester was purchased from Lumiprobe, USA. Cells were cultured in 24-well microplates at  $4 \times 10^5$  cells with plastic coverslips for 24 h. To the wells, 200  $\mu$ M of Cy5-conjugated KBJK557 was added and incubated for 18 h. Coverslips were washed three times with PBS and stained with DAPI for 10 min at room temperature. Subsequently, the coverslips were washed five times again with PBS that was covered with mount solution. Fluorescence images were captured with an inverted Zeiss 710 confocal microscope (Carl Zeiss, Oberkochen, Germany).

**Animals.** Male BALB/c nude mice were purchased from the Nara Bio animal center (NARA Biotech, Seoul, Korea) and housed under specific pathogen-free conditions. The mice were housed in groups of three in transparent plastic cages bedded with aspen chips and were provided with standard mouse chow diet and tap water ad libitum when not being treated. The environment of the animal room was carefully controlled, with a 12 h dark–light cycle. The temperature was maintained at around 20–21 °C with a relative humidity of 40–45%. The animal experiments were carried out according to a protocol approved by the KBSI Committee (KBSI-AEC-1816) and all experiments were performed in accordance with relevant guidelines and regulations.

**Optical Imaging Probe for Tumor Diagnosis.** The xenograft tumor models were prepared by subcutaneous injection of  $4 \times 10^6$  HeLa cancer cells in PBS into the right foreleg region of 5-week-old, male BALB/c nu/nu mice. When the tumor volume reached approximately  $120 \pm 20$  mm<sup>3</sup> at 8 weeks after inoculation, Cy5-conjugated KBJK557 (5 mg/kg body weight/200  $\mu$ L) was injected via the tail vein. Then, to verify that Cy5-conjugated KBJK557 accumulated in the tumor, we carried out *in vivo* fluorescence imaging using the *in vivo* imaging system (IVIS) spectrum (PerkinElmer, USA) at 6, 24, 30, and 48 h with a 640 nm excitation (680, 700, and 720 nm for spectral unmixing) and 680 nm emission filters and a binning factor of 8. Fluorescence was expressed as the average radiance (photons/s/cm<sup>2</sup>/steradian). After *in vivo* scans, the mice were sacrificed by cervical dislocation and tissues of interest (brain, heart, spleen, liver, lung, kidneys, and tumor tissues) were removed immediately. The tissues were scanned using the IVIS Spectrum in the same conditions as *in vivo* scan conditions. ROIs were drawn, such as tumors and other tissues of both *in vivo* imaging and *ex vivo* imaging, and then, the average radiant efficiency of ROIs was measured.

**Anticancer Effect in Tumor-Bearing Mice.** We induced mouse xenograft tumor models by subcutaneously injecting  $2 \times 10^5$  HeLa cells

in PBS into the right thigh region of 5-week-old male BALB/c nu/nu mice. When the tumor volume (length  $\times$  width  $\times$  height, mm<sup>3</sup>) reached approximately 30–40 mm<sup>3</sup>, a tail vein injection of PBS, BI2536, and KBJK557 (5 mg/kg) was carried out. BI2536 and KBJK557 were dissolved in Cremophor EL (Kolliphor EL, Sigma-Aldrich, USA), *N,N*-dimethylacetamide (Sigma-Aldrich, USA), and 2-(hydroxypropyl)- $\beta$ -cyclodextrin (Sigma-Aldrich, USA) (10:10:80, v/v/v, 100  $\mu$ L). We injected PBS, BI2536, and KBJK557 at 3–4-day intervals for 29 days and the tumor size was measured using calipers.

**Pharmacokinetic Profiles of KBJK557.** Male ICR mice were purchased from Koatech, Kyeonggi-do, Korea and were used for the pharmacokinetic study of KBJK557. The blood samples were collected at 0.08, 0.25, 0.5, 1, 2, 4, 6, 8, and 24 h after intravenous administration at a dose of 5 mg/kg in mouse. The blood samples were centrifuged immediately after collection, and the concentrations of the plasma fractions were determined using an Agilent LC–MS/MS system (Agilent, Santa Clara, CA) consisting of an Agilent 1200 series HPLC system connected to an Agilent 6430 mass spectrometer equipped with a turbo electrospray interface. The organ tissues (i.e., liver, spleen, and kidney) were isolated at 2, 6, and 24 h after intravenous administration at a dose of 5 mg/kg into the mouse. After homogenizing the tissues, the concentrations of the tissue were determined as well. The elution was carried out using a linear gradient of 0.1% formic acid in water and 0.1% formic acid acetonitrile (95:5%  $\rightarrow$  5:95%, v/v) at a flow rate of 0.4 mL/min with a reversed-phase high-performance liquid chromatography column (Xterra MS C18, particle size 3.5  $\mu$ m, length and the internal diameter of column 50 mm  $\times$  2.1 mm; Waters, Milford, MA). Multiple reaction monitoring data were collected in positive ionization mode. The samples were monitored at the following Q1/Q3 transitions (*m/z*): 459.2  $\rightarrow$  134 for KBJK557 and 237.0  $\rightarrow$  194.0 for carbamazepine (internal standard). The Agilent software (Data Acquisition and Quantitative Analysis) was used for the operation of the instrument and data collection of KBJK557 and carbamazepine. A noncompartmental analysis was performed to calculate the pharmacokinetic parameters for KBJK557 using the Kinetic software. The area under the plasma concentration–time curve ( $AUC_{last}$ ) was obtained by applying the linear trapezoidal rule. The area under the plasma concentration–time curve from time zero to infinity ( $AUC_{\infty}$ ) was obtained by applying the linear trapezoidal rule with the method of standard area extrapolation. The terminal half-life ( $t_{1/2}$ ) of the compound was calculated by dividing 0.693 with  $\lambda$ , where  $\lambda$  represents the terminal log-linear slope of the KBJK557 concentration–time profile. The total clearance (CL) for KBJK557 was calculated using dose/ $AUC_{\infty}$ , and the steady-state volume of distribution ( $V_{ss}$ ) was then calculated by  $MRT \times CL$ .

## ■ ASSOCIATED CONTENT

### Supporting Information

The Supporting Information is available free of charge at <https://pubs.acs.org/doi/10.1021/acs.jmedchem.0c01451>.

<sup>1</sup>H and <sup>13</sup>C NMR spectra, LC chromatogram, and additional results and schemes (PDF)

Molecular formula strings (CSV)

## ■ AUTHOR INFORMATION

### Corresponding Authors

Kyung S. Lee — Laboratory of Metabolism, Center for Cancer Research, National Cancer Institute, Bethesda, Maryland 20892, United States; [orcid.org/0000-0001-8326-7162](https://orcid.org/0000-0001-8326-7162); Email: [kyunglee@mail.nih.gov](mailto:kyunglee@mail.nih.gov)

Eun Kyong Ryu — Division of Magnetic Resonance, Korea Basic Science Institute (KBSI), Ochang, Chung Buk 28119, Republic of Korea; Department of Bio-analytical Science, University of Science & Technology, Daejeon 34113, Republic of Korea; [orcid.org/0000-0002-8915-2144](https://orcid.org/0000-0002-8915-2144); Email: [ekryu@kbsi.re.kr](mailto:ekryu@kbsi.re.kr)

Jeong Kyu Bang — Division of Magnetic Resonance, Korea Basic Science Institute (KBSI), Ochang, Chung Buk 28119, Republic of

Korea; Department of Bio-analytical Science, University of Science & Technology, Daejeon 34113, Republic of Korea; [orcid.org/0000-0001-5916-0912](https://orcid.org/0000-0001-5916-0912); Phone: +82-43-240-5023; Email: [bangjk@kbsi.re.kr](mailto:bangjk@kbsi.re.kr); Fax: +82-43-240-5059

## Authors

**Pethaiah Gunasekaran** – Division of Magnetic Resonance, Korea Basic Science Institute (KBSI), Ochang, Chung Buk 28119, Republic of Korea; [orcid.org/0000-0001-8436-4183](https://orcid.org/0000-0001-8436-4183)

**Min Su Yim** – Division of Magnetic Resonance, Korea Basic Science Institute (KBSI), Ochang, Chung Buk 28119, Republic of Korea; Department of Bio-analytical Science, University of Science & Technology, Daejeon 34113, Republic of Korea

**Mija Ahn** – Division of Magnetic Resonance, Korea Basic Science Institute (KBSI), Ochang, Chung Buk 28119, Republic of Korea

**Nak-Kyun Soung** – Anticancer Agent Research Center, Korea Research Institute of Bioscience and Biotechnology, Ochang, Chungbuk 28116, Republic of Korea

**Jung-Eun Park** – Laboratory of Metabolism, Center for Cancer Research, National Cancer Institute, Bethesda, Maryland 20892, United States

**Jaehi Kim** – Division of Magnetic Resonance, Korea Basic Science Institute (KBSI), Ochang, Chung Buk 28119, Republic of Korea

**Geul Bang** – Biomedical Omics Group, Korea Basic Science Institute, Ochang, Chung-Buk 363-883, Republic of Korea

**Sang Chul Shin** – Biomedical Research Institute, Korea Institute of Science and Technology, Seoul 02792, Republic of Korea

**Joonhyeok Choi** – Division of Magnetic Resonance, Korea Basic Science Institute (KBSI), Ochang, Chung Buk 28119, Republic of Korea

**Minkyung Kim** – College of Pharmacy, Dongguk University, Goyang 10320, Republic of Korea

**Hak Nam Kim** – Division of Magnetic Resonance, Korea Basic Science Institute (KBSI), Ochang, Chung Buk 28119, Republic of Korea

**Young-Ho Lee** – Division of Magnetic Resonance, Korea Basic Science Institute (KBSI), Ochang, Chung Buk 28119, Republic of Korea; Department of Bio-analytical Science, University of Science & Technology, Daejeon 34113, Republic of Korea; [orcid.org/0000-0002-8441-5814](https://orcid.org/0000-0002-8441-5814)

**Young-Ho Chung** – Drug & Disease Target Research Team, Korea Basic Science Institute (KBSI), Ochang, Chung Buk 28119, Republic of Korea

**Kyeong Lee** – College of Pharmacy, Dongguk University, Goyang 10320, Republic of Korea; [orcid.org/0000-0002-5455-9956](https://orcid.org/0000-0002-5455-9956)

**Eunice EunKyeong Kim** – Biomedical Research Institute, Korea Institute of Science and Technology, Seoul 02792, Republic of Korea

**Young-Ho Jeon** – Laboratory of Biochemistry and Structural Biology, College of Pharmacy, Korea University, Sejong 30019, Republic of Korea

**Min Ju Kim** – Laboratory Animal Resource Center, Korea Research Institute of Bioscience and Biotechnology, Ochang, Chungbuk 28116, Republic of Korea

**Kyeong-Ryoon Lee** – Laboratory Animal Resource Center, Korea Research Institute of Bioscience and Biotechnology, Ochang, Chungbuk 28116, Republic of Korea

**Bo-Yeon Kim** – Anticancer Agent Research Center, Korea Research Institute of Bioscience and Biotechnology, Ochang, Chungbuk 28116, Republic of Korea

Complete contact information is available at:

<https://pubs.acs.org/10.1021/acs.jmedchem.0c01451>

## Author Contributions

††P.G. and M.S.Y. contributed equally to this work.

## Notes

The authors declare no competing financial interest.

## ACKNOWLEDGMENTS

This work was supported by the R&D Convergence Program (CAP-16-03-KRIBB, J.K.B.), the KRIBB Research Initiative Program, and the National Research Foundation of Korea (NRF) grant funded by the Korean government (MSIT) (2020M 3E5E2039159 to Y.H.J., 2020R1A2C1009289 to J.K.B.).

## ABBREVIATIONS

Plk1, polo-like kinase-1; KD, kinase domain; PBD, polo-box domain; SAR, structure–activity relationship; PPG, purpurogallin; DMSO, dimethylsulfoxide; DAPI, 4',6-diamidino-2-phenylindole; WT, wild type; ROI, region of interest; PBS, phosphate-buffered saline; RES, reticulo-endothelial system;  $T_{1/2}$ , half-life; CL, clearance rate; AUC, area under the curve; SD, standard deviation;  $V_{ss}$ , apparent volume of distribution calculated through the steady state; MRT, mean residence time; EDCl, 1-ethyl-3-(3-dimethylaminopropyl)carbodiimide; HOBT, 1-hydroxybenzotriazole; DIEA, *N,N*-diisopropylethylamine; DCM, dichloromethane; MeOH, methanol; TEA, triethylamine; TFA, trifluoroacetic acid; DMF, *N,N*-dimethylformamide; RP HPLC, reversed-phase high-performance liquid chromatography

## REFERENCES

- (1) Park, J.-E.; Soung, N.-K.; Johmura, Y.; Kang, Y. H.; Liao, C.; Lee, K. H.; Park, C. H.; Nicklaus, M. C.; Lee, K. S. Polo-box domain: a versatile mediator of polo-like kinase function. *Cell. Mol. Life Sci.* **2010**, *67*, 1957–1970.
- (2) van Vugt, M. A. T. M.; Medema, R. H. Getting in and out of mitosis with Polo-like kinase-1. *Oncogene* **2005**, *24*, 2844.
- (3) Archambault, V.; Glover, D. M. Polo-like kinases: conservation and divergence in their functions and regulation. *Nat. Rev. Mol. Cell Biol.* **2009**, *10*, 265.
- (4) Petronczki, M.; Lénárt, P.; Peters, J.-M. Polo on the rise—from mitotic entry to cytokinesis with Plk1. *Dev. Cell* **2008**, *14*, 646–659.
- (5) Strebhardt, K. Multifaceted polo-like kinases: drug targets and antitargets for cancer therapy. *Nat. Rev. Drug Discovery* **2010**, *9*, 643.
- (6) Luo, J.; Emanuele, M. J.; Li, D.; Creighton, C. J.; Schlabach, M. R.; Westbrook, T. F.; Wong, K.-K.; Elledge, S. J. A genome-wide RNAi screen identifies multiple synthetic lethal interactions with the Ras oncogene. *Cell* **2009**, *137*, 835–848.
- (7) SpaĚnkuch-Schmitt, B.; Wolf, G.; Solbach, C.; Loibl, S.; Knecht, R.; StegmuĚller, M.; von Minckwitz, G.; Kaufmann, M.; Strebhardt, K. Downregulation of human polo-like kinase activity by antisense oligonucleotides induces growth inhibition in cancer cells. *Oncogene* **2002**, *21*, 3162.
- (8) Steegmaier, M.; Hoffmann, M.; Baum, A.; Lénárt, P.; Petronczki, M.; Krššák, M.; Gürtler, U.; Garin-Chesa, P.; Lieb, S.; Quant, J.; Grauert, M.; Adolf, G. R.; Kraut, N.; Peters, J.-M.; Rettig, W. J. BI 2536, a potent and selective inhibitor of polo-like kinase 1, inhibits tumor growth in vivo. *Curr. Biol.* **2007**, *17*, 316–322.
- (9) Scharow, A.; Raab, M.; Saxena, K.; Sreeramulu, S.; Kudlinzki, D.; Gande, S.; Dötsch, C.; Kurunci-Csacsco, E.; Klaeger, S.; Kuster, B.; Schwalbe, H.; Strebhardt, K.; Berg, T. Optimized Plk1 PBD inhibitors based on poloxin induce mitotic arrest and apoptosis in tumor cells. *ACS Chem. Biol.* **2015**, *10*, 2570–2579.
- (10) Rudolph, D.; Steegmaier, M.; Hoffmann, M.; Grauert, M.; Baum, A.; Quant, J.; Haslinger, C.; Garin-Chesa, P.; Adolf, G. R. BI 6727, a

Polo-like kinase inhibitor with improved pharmacokinetic profile and broad antitumor activity. *Clin. Cancer Res.* **2009**, *15*, 3094–3102.

(11) Lénárt, P.; Petronczki, M.; Steegmaier, M.; Di Fiore, B.; Lipp, J. J.; Hoffmann, M.; Rettig, W. J.; Kraut, N.; Peters, J.-M. The small-molecule inhibitor BI 2536 reveals novel insights into mitotic roles of polo-like kinase 1. *Curr. Biol.* **2007**, *17*, 304–315.

(12) Degenhardt, Y.; Lampkin, T. Targeting Polo-like kinase in cancer therapy. *Clin. Cancer Res.* **2010**, *16*, 384–389.

(13) Davis, M. I.; Hunt, J. P.; Herrgard, S.; Cicceri, P.; Wodicka, L. M.; Pallares, G.; Hocker, M.; Treiber, D. K.; Zarrinkar, P. P. Comprehensive analysis of kinase inhibitor selectivity. *Nat. Biotechnol.* **2011**, *29*, 1046.

(14) Yang, Y.; Bai, J.; Shen, R.; Brown, S. A. N.; Komissarova, E.; Huang, Y.; Jiang, N.; Alberts, G. F.; Costa, M.; Lu, L.; Winkles, J. A.; Dai, W. Polo-like kinase 3 functions as a tumor suppressor and is a negative regulator of hypoxia-inducible factor-1 $\alpha$  under hypoxic conditions. *Cancer Res.* **2008**, *68*, 4077–4085.

(15) Lowery, D. M.; Lim, D.; Yaffe, M. B. Structure and function of Polo-like kinases. *Oncogene* **2005**, *24*, 248.

(16) Lee, K. S.; Grenfell, T. Z.; Yarm, F. R.; Erikson, R. L. Mutation of the polo-box disrupts localization and mitotic functions of the mammalian polo kinase Plk. *Proc. Natl. Acad. Sci. U.S.A.* **1998**, *95*, 9301–9306.

(17) Gheghiani, L.; Loew, D.; Lombard, B.; Mansfeld, J.; Gavet, O. Plk1 activation in late G2 sets up commitment to mitosis. *Cell Rep.* **2017**, *19*, 2060–2073.

(18) Cheng, K.-Y.; Lowe, E. D.; Sinclair, J.; Nigg, E. A.; Johnson, L. N. The crystal structure of the human polo-like kinase-1 polo box domain and its phospho-peptide complex. *EMBO J.* **2003**, *22*, 5757–5768.

(19) Yun, S.-M.; Moulaei, T.; Lim, D.; Bang, J. K.; Park, J.-E.; Shenoy, S. R.; Liu, F.; Kang, Y. H.; Liao, C.; Soung, N.-K.; Lee, S.; Yoon, D.-Y.; Lim, Y.; Lee, D.-H.; Otake, A.; Appella, E.; McMahon, J. B.; Nicklaus, M. C.; Burke Jr, T. R.; Yaffe, M. B.; Wlodawer, A.; Lee, K. S. Structural and functional analyses of minimal phosphopeptides targeting the polo-box domain of polo-like kinase 1. *Nat. Struct. Mol. Biol.* **2009**, *16*, 876.

(20) Liu, F.; Park, J.-E.; Qian, W.-J.; Lim, D.; Gräber, M.; Berg, T.; Yaffe, M. B.; Lee, K. S.; Burke, T. R., Jr. Serendipitous alkylation of a Plk1 ligand uncovers a new binding channel. *Nat. Chem. Biol.* **2011**, *7*, 595.

(21) Ahn, M.; Han, Y.-H.; Park, J.-E.; Kim, S.; Lee, W. C.; Lee, S. J.; Gunasekaran, P.; Cheong, C.; Shin, S. Y.; Kim, H.-Y.; Ryu, E. K.; Murugan, R. N.; Kim, N.-H.; Bang, J. K. A new class of peptidomimetics targeting the polo-box domain of Polo-like kinase 1. *J. Med. Chem.* **2014**, *58*, 294–304.

(22) Reindl, W.; Yuan, J.; Krämer, A.; Strebhardt, K.; Berg, T. Inhibition of polo-like kinase 1 by blocking polo-box domain-dependent protein–protein interaction. *Chem. Biol.* **2008**, *15*, 459–466.

(23) Yuan, J.; Sanhaji, M.; Krämer, A.; Reindl, W.; Hofmann, M.; Kreis, N.-N.; Zimmer, B.; Berg, T.; Strebhardt, K. Polo-box domain inhibitor poloxin activates the spindle assembly checkpoint and inhibits tumor growth in vivo. *Am. J. Pathol.* **2011**, *179*, 2091–2099.

(24) Watanabe, N.; Sekine, T.; Takagi, M.; Iwasaki, J.-i.; Imamoto, N.; Kawasaki, H.; Osada, H. Deficiency in chromosome congression by the inhibition of plk1 polo box domain-dependent recognition. *J. Biol. Chem.* **2009**, *284*, 2344–2353.

(25) Shan, H.-M.; Shi, Y.; Quan, J. Identification of green tea catechins as potent inhibitors of the polo-box domain of polo-like kinase 1. *ChemMedChem* **2015**, *10*, 158–163.

(26) Gali-Muhtasib, H.; Ocker, M.; Kuester, D.; Krueger, S.; El-Hajj, Z.; Diestel, A.; Evert, M.; El-Najjar, N.; Peters, B.; Jurjus, A. Thymoquinone reduces mouse colon tumor cell invasion and inhibits tumor growth in murine colon cancer models. *J. Cell. Mol. Med.* **2008**, *12*, 330–342.

(27) Chen, Y.; Zhang, J.; Li, D.; Jiang, J.; Wang, Y.; Si, S. Identification of a novel polo-like kinase 1 inhibitor that specifically blocks the functions of Polo-Box domain. *Oncotarget* **2017**, *8*, 1234.

(28) Steegmaier, M.; Hoffmann, M.; Baum, A.; Lénárt, P.; Petronczki, M.; Krššák, M.; Gürtler, U.; Garin-Chesa, P.; Lieb, S.; Quant, J.; Grauert, M.; Adolf, G. R.; Kraut, N.; Peters, J.-M.; Rettig, W. J. BI 2536,

a potent and selective inhibitor of polo-like kinase 1, inhibits tumor growth in vivo. *Curr. Biol.* **2007**, *17*, 316–322.

(29) Ma, S.; Liu, M.-A.; Yuan, Y.-L. O.; Erikson, R. L. The serum-inducible protein kinase snk is a G1 phase polo-like kinase that is inhibited by the calcium-and integrin-binding protein CIB1. NIH grant CA42580 and GM59172 (RLE). *Mol. Cancer Res.* **2003**, *1*, 376–384.

(30) Watanabe, N.; Arai, H.; Iwasaki, J.-i.; Shiina, M.; Ogata, K.; Hunter, T.; Osada, H. Cyclin-dependent kinase (CDK) phosphorylation destabilizes somatic wee1 via multiple pathways. *Proc. Natl. Acad. Sci. U.S.A.* **2005**, *102*, 11663–11668.

(31) Elia, A. E. H.; Rellos, P.; Haire, L. F.; Chao, J. W.; Ivins, F. J.; Hoepker, K.; Mohammad, D.; Cantley, L. C.; Smerdon, S. J.; Yaffe, M. B. The molecular basis for phosphodependent substrate targeting and regulation of plks by the polo-box domain. *Cell* **2003**, *115*, 83–95.

(32) Baell, J. B.; Holloway, G. A. New substructure filters for removal of pan assay interference compounds (PAINS) from screening libraries and for their exclusion in bioassays. *J. Med. Chem.* **2010**, *53*, 2719–2740.

(33) Muhamad, N.; Plengsuriyakarn, T.; Na-Bangchang, K. Application of active targeting nanoparticle delivery system for chemotherapeutic drugs and traditional/herbal medicines in cancer therapy: A systematic review. *Int. J. Nanomed.* **2018**, *13*, 3921.

(34) Schmidt, S.; Gonzalez, D.; Derendorf, H. Significance of protein binding in pharmacokinetics and pharmacodynamics. *J. Pharm. Sci.* **2010**, *99*, 1107–1122.

(35) Mastrobattista, E.; Koning, G. A.; Storm, G. Immunoliposomes for the targeted delivery of antitumor drugs. *Adv. Drug Delivery Rev.* **1999**, *40*, 103–127.

(36) Moghimi, S. M.; Hunter, A. C.; Murray, J. C. Long-circulating and target-specific nanoparticles: theory to practice. *Pharmacol. Rev.* **2001**, *53*, 283–318.

(37) Allen, W. J.; Balius, T. E.; Mukherjee, S.; Brozell, S. R.; Moustakas, D. T.; Lang, P. T.; Case, D. A.; Kuntz, I. D.; Rizzo, R. C. DOCK 6: Impact of new features and current docking performance. *J. Comput. Chem.* **2015**, *36*, 1132–1156.

(38) Sterling, T.; Irwin, J. J. ZINC 15—ligand discovery for everyone. *J. Chem. Inf. Model.* **2015**, *55*, 2324–2337.

(39) Qian, W.-J.; Park, J.-E.; Lim, D.; Lai, C. C.; Kelley, J. A.; Park, S.-Y.; Lee, K. W.; Yaffe, M. B.; Lee, K. S.; Burke, T. R., Jr. Mono-anionic phosphopeptides produced by unexpected histidine alkylation exhibit high plk1 polo-box domain-binding affinities and enhanced anti-proliferative effects in hela cells. *Biopolymers* **2014**, *102*, 444–455.